p53-Altered *FBXW7* Expression Determines Poor Prognosis in Gastric Cancer Cases

Takehiko Yokobori,[1,2] Koshi Mimori,[1] Masaaki Iwatsuki,[1] Hideshi Ishii,[1] Ichiro Onoyama,[3] Takeo Fukagawa,[4] Hiroyuki Kuwano,[2] Keiichi I. Nakayama,[3] and Masaki Mori[5]

[1]Department of Surgery, Medical Institute of Bioregulation, Kyushu University, Beppu, Japan; [2]Departments of General Surgical Science, Graduate School of Medicine, Gunma University, Maebashi, Japan; [3]Department of Molecular and Cellular Biology, Medical Institute of Bioregulation, Kyushu University, Fukuoka, Japan; [4]Department of Surgery, National Cancer Center Hospital, Tokyo, Japan; and [5]Department of Gastroenterological Surgery, Graduate School of Medicine, Osaka University, Suita, Japan

Abstract

A molecular target associated with the progression of gastric cancer has not yet been uncovered. *FBXW7* is a tumor suppressor gene transcriptionally controlled by p53 that plays a role in the regulation of cell cycle exit and reentry via c-Myc degradation. Few studies have addressed the clinical significance of *FBXW7* expression in gastric cancer. Therefore, we examined *FBXW7* mRNA expression to determine its clinicopathologic significance in 100 cases of gastric cancer. Low expression levels of *FBXW7* in primary gastric cancer contributed to malignant potential, such as lymph node metastasis ($P = 0.0012$), tumor size ($P = 0.0003$), and poor prognosis ($P = 0.018$). In comparison with 52 cases of gastric cancer without the *p53* mutation, 29 cases with the mutation exhibited lower expression levels of *FBXW7* ($P = 0.0034$), revealing a significant relationship between *p53* mutation and *FBXW7* expression. Furthermore, we found that gastric cancer patients who had low *FBXW7* expression levels and *p53* mutation had a distinctively poor prognosis in comparison with other subgroups ($P = 0.0033$). In conclusion, we showed a role for *p53* in the transcriptional regulation of *FBXW7* expression in clinical gastric cancer cases and showed that disruption of both *p53* and *FBXW7* contributes to poor prognosis. [Cancer Res 2009;69(9):3788–94]

Introduction

FBXW7 is a F-box protein subunit of a SCF-type ubiquitin ligase complex that induces the degradation of positive cell cycle regulators (oncoproteins) such as c-Myc, cyclin E, c-Jun, and Notch. Therefore, *FBXW7* and the associated molecules have been focused on as one of the new carcinoma control structures (1, 2). In particular, *FBXW7* induces cell cycle exit (G_0 phase) via c-Myc degradation, so the altered expression of *FBXW7* is considered one of the major causes of carcinogenesis or carcinoma development (2–4). Because *FBXW7* also participates in cell cycle exit to, and the reentry from, G_0 (5–7), it is a candidate molecular therapeutic target in intractable carcinoma cases that are firmly resistant to combined modality therapies (5, 8).

Mao and colleagues reported that epithelial tumors are not established in $p53^{-/-}$ mice, whereas $p53^{+/-}$ mice form epithelial tumors with altered *FBXW7* expression. *FBXW7* works downstream of *p53*, both of these cell cycle regulator genes, are critical for carcinogenesis of epithelial tissues (3).

Recently, Onoyama and colleagues reported that mice carrying a *FBXW7* T-cell conditional knockout eventually developed thymic lymphomas following thymomas. *FBXW7* and *p53* double-knockout mice developed thymic lymphomas more frequently than other subgroups of knockout mice, such as wild-type, $p53^{-/-}$, and *FBXW7* conditional knockout mice. Therefore, their study clearly showed the consecutive roles of p53 and FBXW7 in the carcinogenesis of solid tumors *in vivo*. Moreover, a comparison of four groups classified according to *FBXW7* and *p53* status revealed a worse prognosis for double inactivation mice than in the other subgroups (6). It is unknown if identical findings were observed during previous *in vivo* studies of human cancer cases.

The clinical significance of *FBXW7* in human solid cancers has been diversely reported. *FBXW7* mutation rates in cholangiocarcinomas, T-cell acute lymphocytic leukemia, endometrial carcinoma, and colorectal cancer were reported as 35%, 31%, 9%, and 9%, respectively (2, 4, 9, 10). Also, *FBXW7* low expression in glioma tissues reportedly produces a poor prognosis (11, 12). Lee and colleagues reported that the *FBXW7* mutation rate in clinical gastric cancer tissues of 3.7% to 6% did not differ in early or progressive gastric cancer (4, 13). However, few studies are available on the connection between *FBXW7* expression level and poor prognoses in gastric cancer.

This study details (*a*) the magnitude of the effect of altered *FBXW7* expression on prognosis determination in gastric cancer cases; (*b*) the significance of both *FBXW7* expression and *p53* mutation status on clinical gastric cancer cases, which was compared with previous *in vivo* reports; and (*c*) how the coexistence of the *p53* mutation and low expression of *FBXW7* in clinical samples determines malignant potential and a poorer prognosis for gastric cancer patients.

Materials and Methods

Clinical samples and cell lines. One hundred gastric cancer samples and paired noncancerous samples were obtained during surgery and used after obtaining informed consent. All patients underwent resection of the primary tumor at Kyushu University Hospital at Beppu and affiliated hospitals between 1992 and 2000. Resected cancer tissues and paired noncancerous tissues were immediately cut and embedded in Tissue-Tek OCT medium (Sakura), frozen in liquid nitrogen, and kept at −80°C until RNA and DNA extraction. Following isolation of RNA and DNA, cDNA was synthesized from 8.0 μg total RNA as described previously (14).

The human gastric cancer cell line AZ521 was provided by the Cell Resource Center of Biomedical Research, Institute of Development, Aging

Note: Supplementary data for this article are available at Cancer Research Online (http://cancerres.aacrjournals.org/).

Requests for reprints: Masaki Mori, Department of Gastroenterological Surgery, Graduate School of Medicine, Osaka University, 2-2 Yamadaoka, Suita 565-0871, Japan. Phone: 81-6-6879-3251; Fax: 81-6-6879-3259; E-mail: mmori@gesurg.med.osaka-u.ac.jp.

doi:10.1158/0008-5472.CAN-08-2846

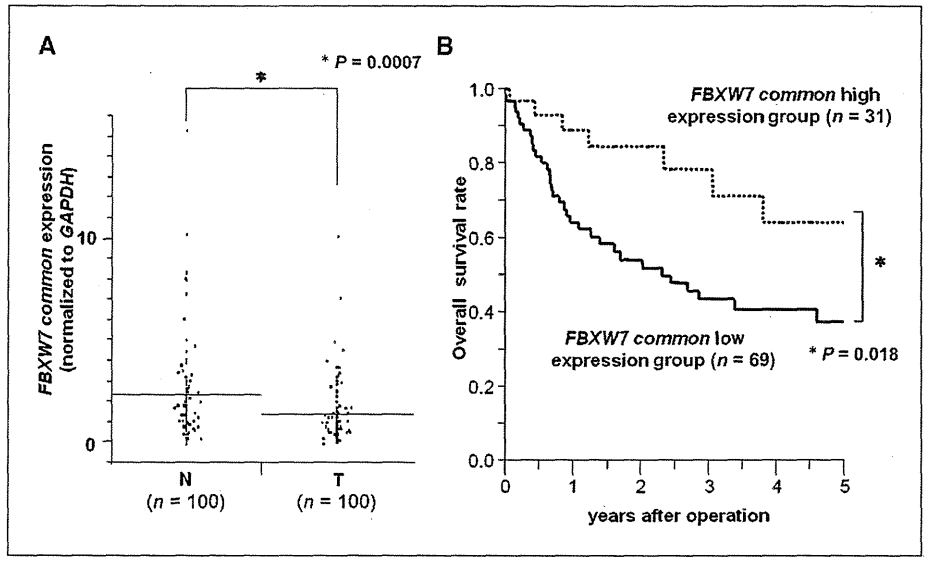

Figure 1. Clinical significance of *FBWX7* mRNA expression in clinical samples. *A*, *FBXW7* mRNA expression in cancer (*T*) and noncancerous (*N*) tissues from gastric cancer patients by real-time reverse transcription-PCR (n = 100). *FBXW7* (T; n = 100), *FBXW7* mRNA (T)/*GAPDH* mRNA (T); *FBXW7* (N; n = 100), *FBXW7* mRNA (N)/*GAPDH* mRNA (N). *Horizontal lines*, mean. *B*, Kaplan-Meier overall survival curves of gastric cancer patients according to the level of *FBXW7* mRNA expression. The high *FBXW7* expression group (n = 31), *FBXW7* (T)/*FBXW7* (N) ≥ 1.0; low *FBXW7* expression group (n = 69), *FBXW7* (T)/*FBXW7* (N) < 1.0.

and Cancer, Tohoku University. This cell line was maintained in RPMI 1640 containing 10% fetal bovine serum with 100 units/mL penicillin and 100 units/mL streptomycin sulfates and cultured in a humidified 5% CO_2 incubator at 37°C.

Real-time quantitative reverse transcription-PCR. *FBXW7*-specific oligonucleotide primers were designed to amplify a 249-bp PCR product encoding the common region among three *FBXW7* isoforms. The following primers were used: *FBXW7* sense primer 5′-AAAGAGTTGTTAGCGGTTCTCG-3′ and antisense primer 5′-CCACATGGATACCATCAAACTG-3′ and glyceraldehyde-3-phosphate dehydrogenase (*GAPDH*; 270 bp) sense primer 5′-GTCAACGGATTTGGTCTGTATT-3′ and antisense primer 5′-AGTCTTCTGGGTGGCAGTGAT-3′. These primers spanned more than two exons to avoid amplification of contaminating genomic DNA. PCR amplification for quantification of *FBXW7* and *GAPDH* mRNA in clinical samples was done in the LightCycler system (Roche Applied Science) using the LightCycler-FastStart DNA Master SYBR Green I Kit (Roche Applied Science) as described previously (15). The amplification conditions of cycles consisted of initial denaturation at 95°C for 10 min followed by 40 cycles of denaturation at 95°C for 10 s, annealing at 62°C (60°C for *GAPDH*) for 10 s, and elongation at 67°C (65°C for *GAPDH*) for 10 s. Melting curve analysis was done to distinguish specific products from nonspecific products and primer dimmers. The relative expression levels of *FBXW7* were obtained by normalizing the amount of *FBXW7* mRNA divided by that of *GAPDH* mRNA as an endogenous control in each sample.

FBXW7 RNA interference. *FBXW7*-specific siRNA (Silencer Predesigned siRNA1: sense GCACAGAAUUGAUACUAACTT and antisense GUUAGUAUCAAUUCUGUGCTG and Silencer Predesigned siRNA2: sense CCUUAUAUGGGCAUACUUCTT and antisense GAAGUAUGCCCAUAUAAGGTG) and negative control siRNA (Silencer Negative Control 1 siRNA) were purchased from Ambion. Lipofectamine RNA interference MAX (Invitrogen) and *FBXW7*-specific siRNA were then added in 6-well flat-bottomed microtiter plates. After incubation, the AZ521 cell line was seeded at 1.5 × 10^5 per well in a volume of 2 mL in 6-well flat-bottomed microtiter plates and incubated in a humidified atmosphere (37°C and 5% CO_2). The RNA interference assay was done after a 24 h incubation.

Immunoblot analysis. Total protein was extracted from AZ521 after *FBXW7* RNA interference. Aliquots of total protein (35 μg) were electrophoresed in 7.5% concentrated READY GELS J (Bio-Rad Laboratories). c-Myc, cyclin E, and p53 proteins were detected using anti-c-Myc (N-262), anti-cyclin E (M-20), and anti-p53 (Pab240; all obtained from Santa Cruz Biotechnology) diluted 1:500, 1:100, and 1:100, respectively. These proteins were normalized to the level of β-actin protein (Cytoskeleton) diluted 1:1,000. Western blot analysis was done as described previously (16). Enhanced chemiluminescence detection reagents (Amersham Biosciences) were used to detect antigen-antibody reactions.

***In vitro* proliferation assay.** Proliferation was determined using the 3-(4,5-dimethylthiazol-2-yl)-2,5-diphenyltetrazolium bromide assay (Roche Diagnostics). After a 24 h incubation following siRNA addition, cells were cultured further for 0 to 72 h and the absorbance of the samples was measured as described previously (17).

***p53* and *FBXW7* sequence.** Among 100 gastric cancer samples in which *FBXW7* mRNA levels were measured, *p53* was sequenced in 81 genomic DNA samples. Similarly, 80 paired cDNA samples were subjected to *FBXW7* mutational analysis.

The 81 genomic DNA samples were used as templates to PCR amplify exons 4 to 9 of the *p53* gene with primers derived from intronic sequences (Supplementary Table S1). The PCR was done with AmpliTaq Gold DNA Polymerase (Applied Biosystems). Likewise, the *FBXW7* (α, β, and γ) sequence was amplified using cDNA from 80 gastric cancer samples with KOD-FX DNA polymerase (TOYOBO) and sequencing primers (Supplementary Table S1). These PCR products were electrophoresed on 1% agarose gels containing ethidium bromide and purified with ethanol precipitation. Purified PCR products were sequenced using a Big-Dye Terminator version 1.1 Cycle Sequencing Kit (Applied Biosystems) and an ABI3100 sequencer (Applied Biosystems).

Statistical analysis. Differences between two groups were estimated with Student's t test, χ^2 analysis, and ANOVA. Overall survival curves were plotted according to the Kaplan-Meier method, with the log-rank test applied for comparison. Survival was measured from the day of the surgery. Data for *FBXW7* mRNA expression levels in three groups were analyzed with ANOVA. When the results of the ANOVA were significant, Tukey's multiple comparison tests were used to assess differences in *FBXW7* mRNA expression levels among each group. All differences were statistically significant at the level of $P < 0.05$ and a tendency was indicated at the level of $P < 0.1$. Statistical analyses were done using the JMP 5 for Windows software package (SAS Institute).

Results

Clinical significance of *FBXW7* mRNA expression in gastric cancer cases. The expression levels of *FBXW7* mRNA in cancerous tissues (n = 100) and paired noncancerous tissues (n = 100) of the gastric cancer patients were examined by real-time reverse transcription-PCR. These data were corrected for *GAPDH* mRNA levels. *FBXW7* mRNA expression levels in cancer

tissues (mean ± SD, 1.41 ± 1.51) were lower than those in noncancerous tissues (2.37 ± 2.3). A significant difference in mRNA mean expression level was found between cancerous and noncancerous tissues (P = 0.0007; Fig. 1*A*). Immunostaining of FBXW7 was done to confirm the correlation between *FBXW7* mRNA and FBXW7 protein. Fifteen gastric cancer samples were divided into two groups according to FBXW7 protein level (high or low). The expression of *FBXW7* mRNA in each group was examined and compared with protein expression levels. The high FBXW7 protein group (n = 7) showed high *FBXW7* mRNA expression levels in comparison with the low FBXW7 protein group (n = 8; P = 0.0013; Supplementary Fig. S1).

In the overall survival curve (Fig. 1*B*), patients in the low *FBXW7* expression group (n = 69; cancer/noncancerous tissues < 1.0) had a significantly poorer prognosis than those in the high *FBXW7* expression group (n = 31; cancer/noncancerous tissues ≥ 1.0; P = 0.018). However, there was no relationship between *FBXW7* expression and clinical stage progression (Supplementary Fig. S2). Multivariate analysis revealed that the *FBXW7* mRNA expression level in cancer is an independent predictor of lymph node metastasis (Supplementary Table S2*A* and B).

Table 1. *FBXW7* gene expression and clinicopathologic factors for 100 gastric cancer patients

	FBXW7/GAPDH		*P*
	High expression (n = 31)	Low expression (n = 69)	
Age (y)			
≥65	15	30	0.69
<65	16	38	
Gender			
Male	17	49	0.12
Female	14	20	
Histology			
Well, moderate	16	34	0.88
Poor, signet	15	34	
Size (cm)			
<5	22	22	0.0003*
≥5	9	47	
Depth			
T_1 (m, sm)	10	11	0.06†
T_2-T_4 (mp, ss, se, si)	21	58	
Lymph node metastasis			
Absent	18	17	0.0012*
Present	13	52	
Lymphatic invasion			
Absent	12	17	0.15
Present	19	52	
Venous invasion			
Absent	27	45	0.024*
Present	4	24	
Liver metastasis			
Absent	31	65	0.17
Present	0	4	
Peritoneal dissemination			
Absent	30	53	0.014*
Present	1	16	
Stage			
I, II	23	28	0.0019*
III, IV	8	41	

NOTE: High *FBXW7* expression group (n = 31), *FBXW7* (T)/*FBXW7* (N) < 1.0; low *FBXW7* expression group (n = 69), *FBXW7* (T)/*FBXW7* (N) < 1.0. Well, well differentiated; poor, poorly differentiated; moderate, moderately differentiated; signet, signet ring cell.
*P < 0.05.
†P < 0.1.

Clinicopathologic factors were significantly different in the low *FBXW7* expression group (n = 69). There was more progressive tumor size, lymph node metastasis, venous invasion, peritoneal dissemination, and clinical staging compared with the high *FBXW7* expression group (n = 31; P < 0.05). However, no significant differences were observed regarding age, gender, histology, lymphatic invasion, and liver metastasis (Table 1).

Expression of the *FBXW7* isoform and prognosis in gastric cancer cases. In several *in vivo* studies, mouse *Fbxw7* has three isoforms (α, β, and γ). The α isoform is expressed in most tissues, the β isoform is found in the brain and testis, and the γ isoform is in the heart and muscle (5). We confirmed the distribution of *FBXW7* expression in a human panel before searching for *FBXW7* mutations in gastric cancer cases. We found a similar distribution of *FBXW7* mRNA expression between the human panel and laboratory mice (Supplementary Fig. S3). *Fbxw7* γ controls the nucleolar level of c-Myc and cell size and is restricted to muscle cells, which is larger than other cells (5, 18). It has been suggested that *Fbxw7* γ contributes to muscle differentiation through regulation of c-Myc. Therefore, the expression level of *FBXW7* γ in the heart might be very high to regulate heart muscle differentiation (Supplementary Fig. S3).

In addition, the association between overall *FBXW7* expression and poor prognosis was more significant than between the expression of any individual isoform (Supplementary Fig. S4).

***FBXW7* and *p53* mutation analysis.** We examined *p53* mutations in 81 genomic DNA samples and *FBXW7* mutations in 80 cDNA samples, the same paired samples that were used for the *FBXW7* mRNA expression assay. Mutation analysis done with sequencing found *p53* and *FBXW7* mutation rates of 35.8% (29 of 81) and 8.8% (7 of 80), respectively (Fig. 2*A* and *B*; Supplementary Table S3; Supplementary Fig. S5).

Examination of the relationship between *p53* mutation status and *FBXW7* mRNA expression levels revealed that *FBXW7* mRNA mean expression levels in the *p53* mutation (+) group (n = 29; 1.07 ± 1.03) were lower than those in the *p53* mutation (−; n = 52; 1.56 ± 1.79) and noncancerous tissues (n = 100; 2.36 ± 2.3). A significant difference was found between the *p53* mutation (+) group and the other groups (Fig. 3). In addition, no difference was observed between the *p53* mutation (−) gastric cancer tissues and noncancerous tissues.

Mean expression levels of *FBXW7* in the *FBXW7* mutation (+) group (n = 7) were not significantly different from those of the *FBXW7* mutation (−) group (n = 73) and noncancerous tissues (n = 100). The presence of the *FBXW7* mutation was not associated with poor prognosis or clinical stage in gastric cancer patients (Supplementary Fig. S5).

***FBXW7* RNA interference promotes proliferation *in vitro*.** Because *FBXW7* mRNA suppression in cancer tissues is associated with poor prognosis, the protein levels of c-Myc and cyclin E, degradation targets of *FBXW7*, were examined to evaluate *FBXW7* function in gastric cancer cells. *FBXW7*

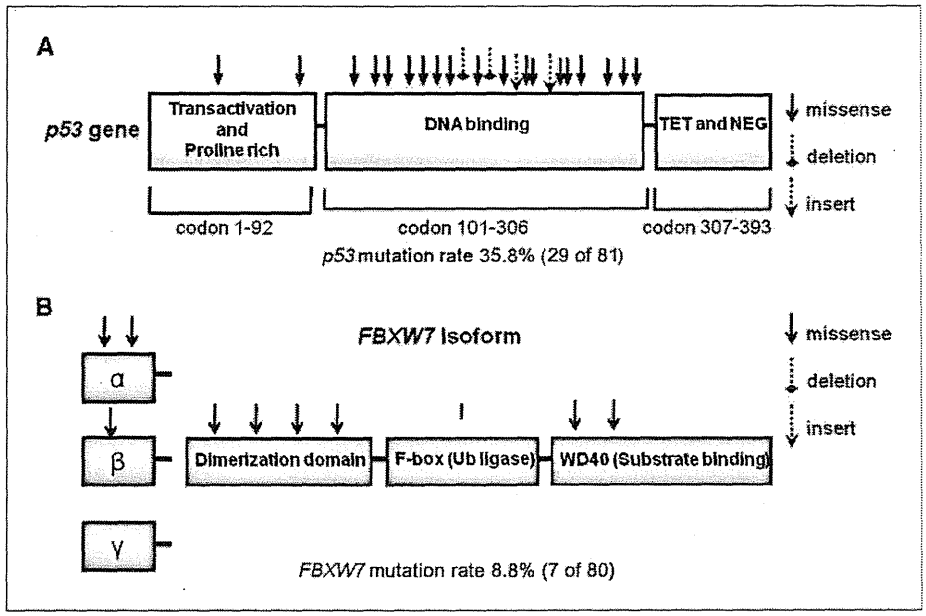

Figure 2. *p53* and *FBXW7* mutation analysis. *A*, structure and mutation of the *p53* gene in gastric cancer patients ($n = 81$). *B*, structure and mutation of the *FBXW7* gene in gastric cancer patients ($n = 80$). *Arrows*, mutation type, such as missense, deletion, and insertion.

suppression analysis was done with two different *FBXW7* siRNA (siRNA1 or siRNA2) using gastric cancer cell line AZ521. *FBXW7* suppression by siRNA was confirmed with quantitative reverse transcription-PCR in the control siRNA and *FBXW7* siRNA groups. The level of *FBXW7* mRNA was substantially reduced by 70% in *FBXW7* siRNA1 (Fig. 4*A*).

Western blot analysis confirmed expression of c-Myc and cyclin E proteins degradation targets of *FBXW7* in control siRNA and *FBXW7* siRNA groups. The expression levels of c-Myc and cyclin E protein were enhanced in the *FBXW7* siRNA group compared with the control siRNA group. Likewise, p53 expression was enhanced (Fig. 4*B*). Evaluation of proliferation potency in the *FBXW7* siRNA groups using the 3-(4,5-dimethylthiazol-2-yl)-2,5-diphenyltetrazolium bromide assay showed that proliferation rates were significantly enhanced in both *FBXW7* groups in comparison with the control siRNA group and parent cell line AZ521 (Fig. 4*C*).

***p53* mutation and *FBXW7* expression are associated with poor prognosis in clinical gastric cancer patients.** *FBXW7* mRNA expression was inhibited in *p53* mutation (+) gastric cancer tissues, and the low *FBXW7* expression patients had a significantly poorer prognosis than the high *FBXW7* expression patients (Figs. 1*B* and 3).

Therefore, we divided 81 gastric cancer patients into four groups according to *FBXW7* expression level and the state of the *p53* mutation and examined the overall survival curve in these groups. The *p53* mutation (+), *FBXW7* low expression group ($n = 24$) had a significantly poorer prognosis than the other three groups ($P = 0.0033$; Fig. 5).

Discussion

In this study, we showed that *FBXW7* mRNA expression in gastric cancer samples is markedly decreased in comparison with the corresponding noncancerous samples and that *FBXW7* is a poor prognostic factor. There are three possible explanations. First, it is worth noting that *FBXW7* expression is regulated by p53 in *in vitro* and *in vivo* experimental data (3, 5, 6, 19). For instance, Mao and colleagues reported that *Fbxw7* mRNA expression was activated when *p53* expression was induced by radiation, and baseline expression of *Fbxw7* mRNA is suppressed in $p53^{-/-}$ mice. Moreover, they reported that a p53-binding site is present in a promoter region of the mouse *Fbxw7* (3). In addition, Kimura and colleagues reported that *FBXW7* β expression is enhanced when wild-type *p53* is produced in a *p53*-mutated glioblastoma cell line (8). These reports strongly suggest that transcription of *FBXW7* is regulated by p53 activity. Therefore, we focused on the regulation of *FBXW7* expression by p53 in gastric cancer cases. In the current study, *FBXW7* expression levels were decreased in most *p53* mutation (+) gastric cancer samples (Fig. 3); only 6% (5 of 81) cases were *FBXW7* high expression in *p53* mutation (+; Fig. 5). Most of the p53 mutation (+) gastric cancer patients belonged to the *FBXW7* low expression group. Therefore, we propose that *FBXW7* mRNA expression is primarily regulated by the presence of the *p53* mutation in clinical gastric cancer cases. It is worth noting that the reproducibility of this finding *in vivo* was clearly confirmed in human clinical cases. To determine which isoform of *FBXW7* is regulated by p53 *in vitro*, we used *p53* siRNA to suppress *p53* expression in gastric cancer cell line AZ521. The expression levels of the three *FBXW7* isoforms (α, β, and γ) were suppressed by *p53* siRNA (Supplementary Fig. S6).

Second, we determined that *FBXW7* is inactivated by a mutation in the coding region. The average of *FBXW7* mutation rate in several malignancies was ~6% (4). As for gastric cancer cases, Lee and colleagues reported the possibility of the presence of mutation, but the relationship of the *FBXW7* mutation and prognosis was not elucidated (13). Therefore, we examined the sequence of the *FBXW7* isoforms. The *FBXW7* mutation rate, 8.8% (7 of 80), was similar to the 3.7% to 6% previously reported for gastric cancer (4, 13). Mutation hotspots are located in T-cell acute lymphocytic leukemia; however, they were not detected in the current study (13, 20, 21).

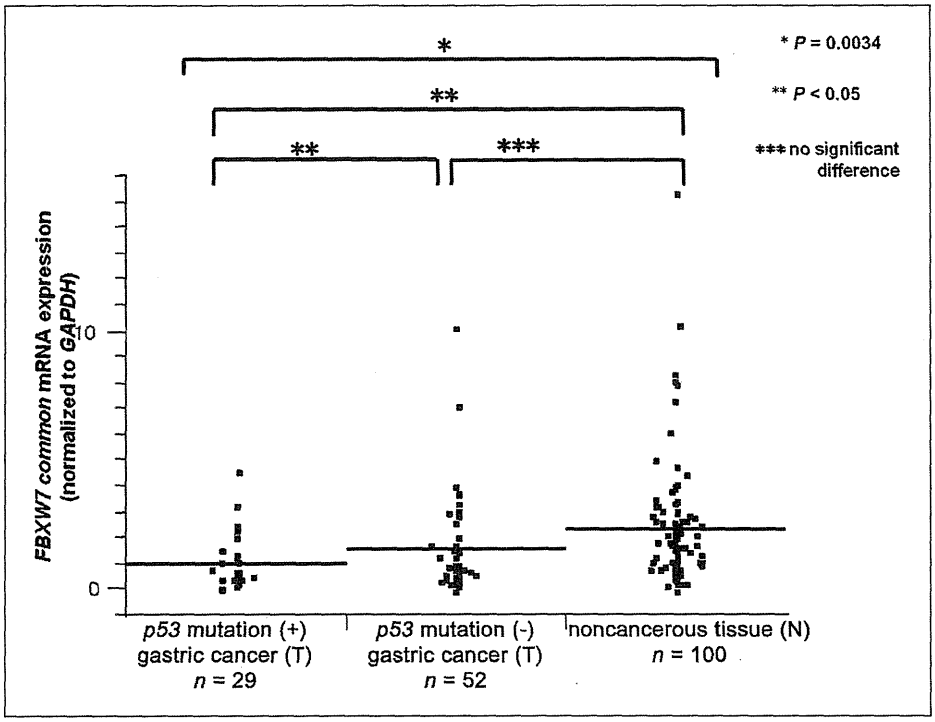

Figure 3. Relationship between *FBXW7* mRNA expression and *p53* mutation. Gastric cancer patients were divided into two groups based on the presence or absence of the *p53* mutation. The two groups were the *p53* mutation (+) gastric cancer group (n = 29) and the *p53* mutation (−) gastric cancer group (n = 52). *FBXW7* expression levels in *p53* mutation (+) patients were lower than in the other groups. *Horizontal lines,* mean expression value of each group. The statistical analysis for comparisons was done in the order of ANOVA and Tukey's test.

Third, chromosome 4q contains the *FBXW7* gene. Approximately 30% of the gene is deleted in certain carcinomas, such as esophageal and gastric cancers. In particular, inactivation of tumor suppressor genes by the chromosome 4q deletion may be an important factor in colon carcinogenesis (22–24).

The reduction of *FBXW7* expression is associated with the dysregulation of cyclin E and c-Myc, positive regulators of the cell cycle (2, 18, 25, 26). c-Myc is associated with cell growth and is recognized as an important factor in control of the G_1 (G_0) to S-phase transition (1, 6, 27, 28). Cyclin E expression is enhanced in various types of cancer, where it regulates cell cycle progression via Rb phosphorylation and contributes to genome instability (19, 29). Consistent with previously published reports, we showed that protein expression of c-Myc and cyclin E is enhanced when *FBXW7* is suppressed in a gastric cancer cell line (Fig. 4). Immunohistochemical analysis of FBXW7 in clinical gastric cancer tissues revealed enhanced expression of Myc and cyclin E in FBXW7 low expression tissues (Supplementary Fig. S7*A*). Conversely, Myc and

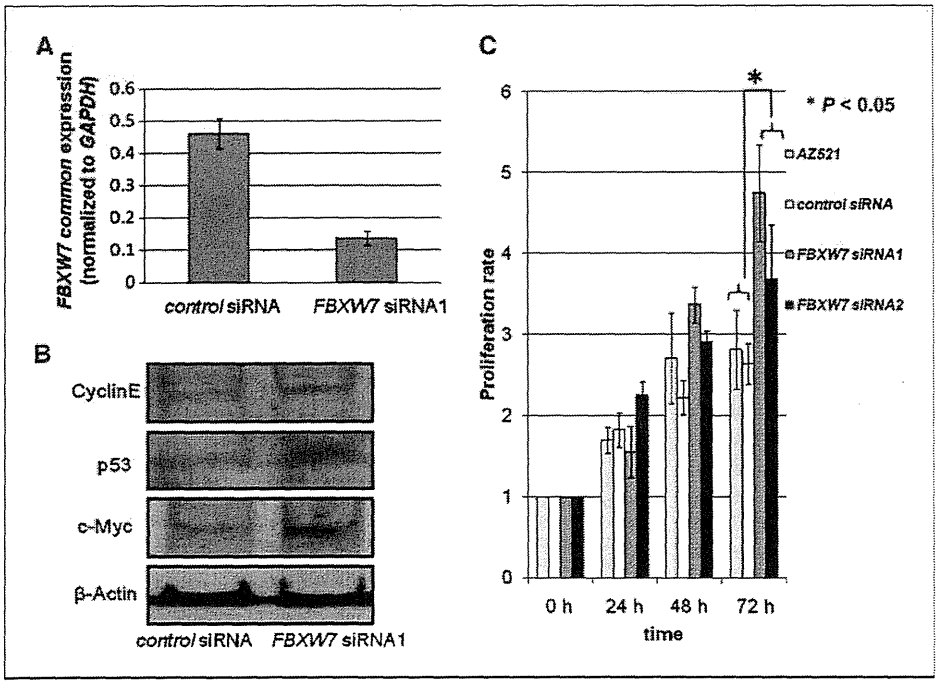

Figure 4. Proliferation assay with RNA interference of *FBXW7* in the AZ521 gastric cancer cell line. *A,* reduced *FBXW7* expression was confirmed by quantitative reverse transcription-PCR analyses in *FBXW7* siRNA1 cells compared with control siRNA. *FBXW7* expressions were normalized by *GAPDH* expression. Mean ± SD. *B,* Western blot analysis of c-Myc, cyclin E, and p53 in *FBXW7* siRNA cells and control siRNA cells. These proteins were normalized to the level of β-actin. *C,* 3-(4,5-dimethylthiazol-2-yl)-2,5-diphenyltetrazolium bromide assay. The proliferation rate of *FBXW7* siRNA (1 and 2) cells was enhanced over that of control siRNA and parent AZ521 cells. Mean ± SD.

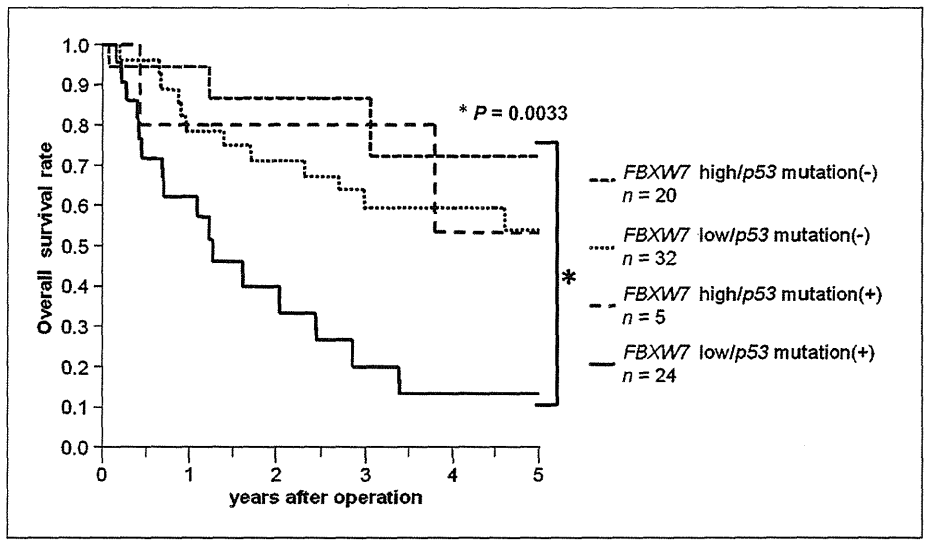

Figure 5. Kaplan-Meier overall survival curves of gastric cancer patients based on *FBXW7* mRNA expression and *p53* mutation. The survival rate for patients in the low *FBXW7* expression and *p53* mutation (+) group was significantly lower than that for patients in the other three groups ($P < 0.05$): high *FBXW7* expression and *p53* mutation (−; $n = 20$), high *FBXW7* expression and *p53* mutation (+; $n = 5$), low *FBXW7* expression and *p53* mutation (−; $n = 32$), and low *FBXW7* expression and *p53* mutation (+; $n = 24$).

cyclin E expression levels were suppressed in tissues in which FBXW7 was overexpressed (Supplementary Fig. S7*B*), confirming the relationship between FBXW7 and target proteins in clinical gastric cancer tissues.

In addition, c-Myc accumulation induces p53-dependent apoptosis via MDM2 degradation (6, 30, 31). The inactivation of both *FBXW7* and *p53* promotes c-Myc accumulation and inhibits p53-dependent apoptosis by MDM2 activation. It probably means that the proliferation rate was increased in these cells.

The low *FBXW7* expression group of gastric cancer patients showed progression of clinicopathologic factors and poor prognosis. All 4 cases of liver metastasis (100%, 4 of 4), 16 cases of peritoneal dissemination (94%, 16 of 17), and 24 cases of venous invasion (86%, 24 of 28) were classified as members of the *FBXW7* low expression group (Table 1). Unfortunately, a significant correlation was not observed between the incidence of liver metastasis and *FBXW7* expression because of an insufficient number of cases. However, other clinicopathologic findings indicated that FBXW7 contributes to hematogenous metastasis besides lymph node metastasis and peritoneal dissemination.

FBXW7 is a tumor suppressor. Considering tumor dormancy as one way to conquer malignancies, the introduction of FBXW7 may facilitate "tumor dormancy therapy." Moreover, it was found that Myc inhibition triggers rapid regression of incipient and established lung tumors *in vivo* (32). Therefore, Myc degradation by FBXW7 may not only induce a state of tumor dormancy but also could have an antitumor effect.

As in a previous *in vivo* study, the simultaneous disruption of two cell cycle checkpoint genes, *p53* and *FBXW7*, shortened the survival of mice with thymic lymphomas (6). It is notable that, even in the *FBXW7* low expression group, the 5-year survival rate of *p53* mutation (−) cases is 53%, but we found that it was 14% in the *FBXW7* low expression/*p53* mutation (+) group of clinical gastric cancer patients (Fig. 5). Both *p53* and *FBXW7* act to brake the cell cycle. Therefore, simultaneous disruption of these genes led to poor prognosis in clinical gastric cancer in comparison with inactivation of *p53* or *FBXW7* alone. Although p53 reportedly regulates *FBXW7* expression, other mechanisms may be present. In the current study, most cases of *p53* mutation (+) gastric cancer were in the low *FBXW7* group and had poor prognosis (83%, 24 of 29). However, a few cases of *p53* mutation (+) gastric cancer were in the high *FBXW7* expression group (17%, 5 of 29) and had good prognosis in comparison with the *p53* mutation (+)/low *FBXW7* group. There were a few cancer cases with higher *FBXW7* expression that was not regulated by p53. Therefore, the prognosis of *p53* mutation (+) cases is not identical to that of *p53* mutation (+)/*FBXW7* low cases.

These results show that the status of *FBXW7* and *p53* is critical for prognosis determination in gastric cancer patients. This report is the first confirmation of the experimental mice data using clinical gastric cancer samples.

In conclusion, *FBXW7* has recently attracted attention as a tumor suppressor gene that reduces important oncoproteins and related carcinogenesis and cell cycle progression. There are previous reports of *in vitro* and *in vivo* studies showing that p53 controls *FBXW7* expression and that *FBXW7* inactivation contributes to poor prognosis via genome instability and cell cycle progression. However, these findings had not been shown in clinical cancer samples. We have clarified that gastric cancer patients with inactivation of *FBXW7* and *p53* have a poorer prognosis.

Disclosure of Potential Conflicts of Interest

No potential conflicts of interest were disclosed.

Acknowledgments

Received 8/5/08; revised 2/2/09; accepted 2/25/09; published OnlineFirst 4/14/09.

Grant support: CREST, Japan Science and Technology Agency; Japan Society for the Promotion of Science Grant-in-Aid for Scientific Research grants 17109013, 18659384, 18390367, 18590333, 18015039, 19591509, 19390336, 20390360, 20591547, 20790961, 20659209, and 20790960; The Ministry of Education, Culture, Sports, Science and Technology Grant-in-Aid for Scientific Research on Priority Areas grant 18015039; Third-Term Comprehensive 10-Year Strategy for Cancer Control grant 16271201; New Energy and Industrial Technology Development Organization Technological Development for Chromosome Analysis; The Ministry of Education, Culture, Sports, Science and Technology of Japan for Scientific Research on Priority Areas, Cancer Translational Research Project; and Grant of Clinical Research Foundation 2008-2010.

The costs of publication of this article were defrayed in part by the payment of page charges. This article must therefore be hereby marked *advertisement* in accordance with 18 U.S.C. Section 1734 solely to indicate this fact.

We thank T. Shimooka, K. Ogata, M. Kasagi, Y. Nakagawa, and T. Kawano for technical assistance.

References

1. Nakayama KI, Nakayama K. Ubiquitin ligases: cell-cycle control and cancer. Nat Rev Cancer 2006;6:369–81.
2. Welcker M, Clurman BE. FBW7 ubiquitin ligase: a tumour suppressor at the crossroads of cell division, growth and differentiation. Nat Rev Cancer 2008;8:83–93.
3. Mao JH, Perez-Losada J, Wu D, et al. Fbxw7/Cdc4 is a p53-dependent, haploinsufficient tumour suppressor gene. Nature 2004;432:775–9.
4. Akhoondi S, Sun D, von der Lehr N, et al. FBXW7/hCDC4 is a general tumor suppressor in human cancer. Cancer Res 2007;67:9006–12.
5. Matsumoto A, Onoyama I, Nakayama KI. Expression of mouse Fbxw7 isoforms is regulated in a cell cycle- or p53-dependent manner. Biochem Biophys Res Commun 2006;350:114–9.
6. Onoyama I, Tsunematsu R, Matsumoto A, et al. Conditional inactivation of Fbxw7 impairs cell-cycle exit during T cell differentiation and results in lymphomatogenesis. J Exp Med 2007;204:2875–88.
7. Matsuoka S, Oike Y, Onoyama I, et al. Fbxw7 acts as a critical fail-safe against premature loss of hematopoietic stem cells and development of T-ALL. Genes Dev 2008;22:986–91.
8. Kimura T, Gotoh M, Nakamura Y, Arakawa H. hCDC4b, a regulator of cyclin E, as a direct transcriptional target of p53. Cancer Sci 2003;94:431–6.
9. Nakayama KI, Nakayama K. Regulation of the cell cycle by SCF-type ubiquitin ligases. Semin Cell Dev Biol 2005;16:323–33.
10. Yan T, Wunder JS, Gokgoz N, Seto KK, Bell RS, Andrulis IL. hCDC4 variation in osteosarcoma. Cancer Genet Cytogenet 2006;169:138–42.
11. Hagedorn M, Delugin M, Abraldes I, et al. FBXW7/hCDC4 controls glioma cell proliferation *in vitro* and is a prognostic marker for survival in glioblastoma patients. Cell Div 2007;2:9.
12. Bredel M, Bredel C, Juric D, et al. Functional network analysis reveals extended gliomagenesis pathway maps and three novel MYC-interacting genes in human gliomas. Cancer Res 2005;65:8679–89.
13. Lee JW, Soung YH, Kim HJ, et al. Mutational analysis of the hCDC4 gene in gastric carcinomas. Eur J Cancer 2006;42:2369–73.
14. Enders GH. Cyclins in breast cancer: too much of a good thing. Breast Cancer Res 2002;4:145–7.
15. Ogawa K, Utsunomiya T, Mimori K, et al. Clinical significance of human kallikrein gene 6 messenger RNA expression in colorectal cancer. Clin Cancer Res 2005;11:2889–93.
16. Ieta K, Ojima E, Tanaka F, et al. Identification of overexpressed genes in hepatocellular carcinoma, with special reference to ubiquitin-conjugating enzyme E2C gene expression. Int J Cancer 2007;121:33–8.
17. Ieta K, Tanaka F, Utsunomiya T, Kuwano H, Mori M. CEACAM6 gene expression in intrahepatic cholangiocarcinoma. Br J Cancer 2006;95:532–40.
18. Welcker M, Orian A, Grim JE, Eisenman RN, Clurman BE. A nucleolar isoform of the Fbw7 ubiquitin ligase regulates c-Myc and cell size. Curr Biol 2004;14:1852–7.
19. Minella AC, Grim JE, Welcker M, Clurman BE. p53 and SCF(Fbw7) cooperatively restrain cyclin E-associated genome instability. Oncogene 2007;26:6948–53.
20. Malyukova A, Dohda T, von der Lehr N, et al. The tumor suppressor gene hCDC4 is frequently mutated in human T-cell acute lymphoblastic leukemia with functional consequences for Notch signaling. Cancer Res 2007;67:5611–6.
21. Tan Y, Sangfelt O, Spruck C. The Fbxw7/hCdc4 tumor suppressor in human cancer. Cancer Lett 2008;271:1–12.
22. Sterian A, Kan T, Berki AT, et al. Mutational and LOH analyses of the chromosome 4q region in esophageal adenocarcinoma. Oncology 2006;70:168–72.
23. Sundqvist A, Bengoechea-Alonso MT, Ye X, et al. Control of lipid metabolism by phosphorylation-dependent degradation of the SREBP family of transcription factors by SCF(Fbw7). Cell Metab 2005;1:379–91.
24. Takada H, Imoto I, Tsuda H, et al. Screening of DNA copy-number aberrations in gastric cancer cell lines by array-based comparative genomic hybridization. Cancer Sci 2005;96:100–10.
25. Welcker M, Orian A, Jin J, et al. The Fbw7 tumor suppressor regulates glycogen synthase kinase 3 phosphorylation-dependent c-Myc protein degradation. Proc Natl Acad Sci U S A 2004;101:9085–90.
26. Welcker M, Singer J, Loeb KR, et al. Multisite phosphorylation by Cdk2 and GSK3 controls cyclin E degradation. Mol Cell 2003;12:381–92.
27. Spencer CA, Groudine M. Control of c-myc regulation in normal and neoplastic cells. Adv Cancer Res 1991;56:1–48.
28. Onoyama I. Cyclin E and c-Myc degradation by SCF(Fbxw7). Tanpakushitsu Kakusan Koso 2006;51:1382–5.
29. Ji P, Zhu L. Using kinetic studies to uncover new Rb functions in inhibiting cell cycle progression. Cell Cycle 2005;4:373–5.
30. Zindy F, Eischen CM, Randle DH, et al. Myc signaling via the ARF tumor suppressor regulates p53-dependent apoptosis and immortalization. Genes Dev 1998;12:2424–33.
31. Pelengaris S, Khan M. The many faces of c-MYC. Arch Biochem Biophys 2003;416:129–36.
32. Soucek L, Whitfield J, Martins CP, et al. Modelling Myc inhibition as a cancer therapy. Nature 2008;455:679–83.

Defined factors induce reprogramming of gastrointestinal cancer cells

Norikatsu Miyoshi[a], Hideshi Ishii[a,b,1], Ken-ichi Nagai[a], Hiromitsu Hoshino[a], Koshi Mimori[b], Fumiaki Tanaka[b], Hiroaki Nagano[a], Mitsugu Sekimoto[a], Yuichiro Doki[a], and Masaki Mori[a,b,1]

[a]Department of Gastroenterological Surgery, Osaka University Graduate School of Medicine, Osaka 565-0871, Japan; and [b]Department of Molecular and Cellular Biology, Division of Molecular and Surgical Oncology, Medical Institute of Bioregulation, Kyushu University, Ohita 874-0838, Japan

Communicated by Takashi Sugimura, National Cancer Center, Tokyo, Japan, November 4, 2009 (received for review August 11, 2009)

Although cancer is a disease with genetic and epigenetic origins, the possible effects of reprogramming by defined factors remain to be fully understood. We studied the effects of the induction or inhibition of cancer-related genes and immature status-related genes whose alterations have been reported in gastrointestinal cancer cells. Retroviral-mediated introduction of induced pluripotent stem (iPS) cell genes was necessary for inducing the expression of immature status-related proteins, including Nanog, Ssea4, Tra-1-60, and Tra-1-80 in esophageal, stomach, colorectal, liver, pancreatic, and cholangiocellular cancer cells. Induced cells, but not parental cells, possessed the potential to express morphological patterns of ectoderm, mesoderm, and endoderm, which was supported by epigenetic studies, indicating methylation of DNA strands and the histone H3 protein at lysine 4 in promoter regions of pluripotency-associated genes such as *NANOG*. In in vitro analysis induced cells showed slow proliferation and were sensitized to differentiation-inducing treatment, and in vivo tumorigenesis was reduced in NOD/SCID mice. This study demonstrated that pluripotency was manifested in induced cells, and that the induced pluripotent cancer (iPC) cells were distinct from natural cancer cells with regard to their sensitivity to differentiation-inducing treatment. Retroviral-mediated introduction of iPC cells confers higher sensitivity to chemotherapeutic agents and differentiation-inducing treatment.

cancer stem cells | epigenetics | pluripotent stem cells | embryonic stem cells | differentiation

Cancer is thought to be a genetic and epigenetic disease with uncontrolled proliferative potential. Although the idea was proposed decades ago, the concept that some cancer cells arise from small populations, termed cancer stem cells (CSCs), with both self-renewal potential and multipotential properties sufficient to form tumors, has emerged recently (1, 2). This small population of CSCs possesses persistent self-renewal potential that can be detected by various in vitro assessments and in vivo animal experiments (2). Therefore, it has been proposed that malignant tumors are derived from CSCs with uncontrolled proliferative potential and dysregulation of their mechanisms of differentiation (2).

The origins of CSCs remain incompletely understood (1–3). One view is that CSCs are formed as a result of alterations arising in cells that have already differentiated (1); alternatively, another notion holds that their generation is a result of tumorigenesis that has occurred in immature tissue stem cells or progenitor cells (2); however, in both theories, epigenetic organization participates in tumorigenic regulation (1, 2).

With the investigation and development of ES cells from zygote to blastodermic vesicle stages, the elucidation of the molecular mechanisms that specify pluripotent differentiation has made remarkable progress (4, 5). Regarding the regulation of molecular mechanisms managing this pluripotency, it is obvious that several types of transcription factors specifically discovered in multipotential stem cells display mutual cooperation as a result of epigenetic controls (6–9).

In this study, we analyzed the effects of transcription factor genes that were previously reported in induced pluripotent stem (iPS) cells (6, 7), as well as cancer-related oncogenes and tumor suppressor genes. The repression of tumor-suppressor genes extends the lifespan of embryonic stem (ES) cells or increases the induction efficiency of iPS cells and maintains their immortalized state (10–12). The results indicated that introduction of transcription factor genes into gastrointestinal cancer cells resulted in reprogramming of cells to a pluripotent state and sensitized them to differentiation induction. Such reprogrammed cells were distinct from parental cells. It is hoped that the generation of induced pluripotent cancer (iPC) cells will eventually accomplish some goals in this field. One such goal is the inspection of previously uncharacterized cancer treatments using differentiation therapy via the induction of drug susceptibility in cancer cells. Reprogramming of cancer cells supports the notion that transduction might cause differentiation of cells to unique cell lineages. Another goal is the exploitation of drug discoveries with the aim of producing therapeutic and diagnostic reagents and using them in their clinical applications.

Results

Expression of Genes Inducing Immature Status in Gastrointestinal Cancer Cell Lines. We performed quantitative real-time reverse transcription PCR (RT-PCR) analysis on 20 gastrointestinal cancer cell lines by using immature status-related gene primers for *NANOG, OCT3/4, SOX2, KLF4,* and *LIN28* (Fig. S1*A*). From the results of RT-PCR analysis, we selected cancer cell lines such as DLD-1, HCT116, MIAPaCa-2, and PLC, which exhibited relatively low *NANOG* mRNA expression. In these cells, immature status seems to be effectively exhibited and represented as high *NANOG* expression (6–9). Especially in the colorectal cancer cell line DLD-1, all five selected genes showed relatively low expression compared to the other gastrointestinal cancer cell lines. We then studied the induction of simultaneous combinations of several factors, which include *OCT3/4, SOX2, KLF4,* and *c-MYC,* as well as oncogenes (*BCL2* and *KRAS*) and tumor suppressor genes shRNA (*TP53, P16(INK4A), PTEN, FHIT, RB1*) (Fig. S1 *B* and *C*). These factors were transfected into four cancer cell lines with ecotropic retrovirus produced in PLAT-E packaging cells. Four transcription factors *OCT3/4, SOX2, KLF4,* and *c-MYC* significantly induced up-regulation of *NANOG* mRNA.

Induction of ES-Like State Cancer Cells with Lentiviral and Retroviral Transduction. Induction of human cancer cell lines using lentiviruses and retroviruses requires high transduction efficiencies. We optimized the transduction methods for cancer cell lines (Fig. 1*A*). The four transcription factors, *OCT3/4, SOX2, KLF4,* and *c-MYC,* were transfected into cancer cell lines with ecotropic retrovirus

Author contributions: N.M., H.I., and M.M. designed research; N.M. performed research; N.M. and H.I. contributed new reagents/analytic tools; N.M., H.I., K.N., H.H., K.M., F.T., H.N., M.S., Y.D., and M.M. analyzed data; and N.M. wrote the paper.

The authors declare no conflict of interest.

[1]To whom correspondence may be addressed. E-mail: hishii@gesurg.med.osaka-u.ac.jp or mmori@gesurg.med.osaka-u.ac.jp.

This article contains supporting information online at www.pnas.org/cgi/content/full/0912407107/DCSupplemental.

www.pnas.org/cgi/doi/10.1073/pnas.0912407107

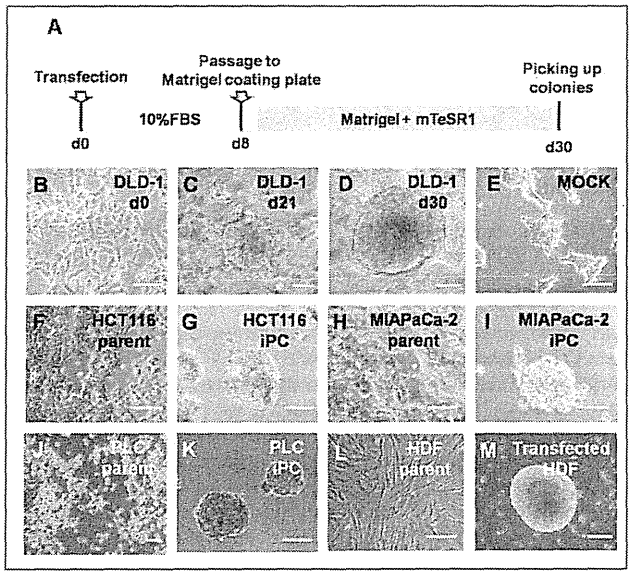

Fig. 1. Induction of human cancer cells with retroviral transduction. (*A*) We optimized the time course of the induction from human cancer cells; the schedule is summarized. (*B–E*) DLD-1 morphology was exhibited. Twenty days later, we observed distinct types of colonies with round shapes (*C* and *D*) that were different from the wild type (*B*). (*E*) Mock was transfected with pMXs Retroviral Vector as a negative control . (*F–K*) Parental and iPC cells of gastrointestinal cancer cell lines from HCT116 (*F* and *G*), MIAPaCa-2 (*H* and *I*), and PLC (*J* and *K*). (*L* and *M*) The referential morphologies are exhibited by HDF. Scale bar: 200 μm. (Original magnification, ×200)

produced in PLAT-E packaging cells. Eight days after transduction, the cells were harvested by trypsinization and plated onto Matrigel-coated plates. The next day, the Dulbecco's modified Eagle medium (DMEM) containing 10% FBS was replaced with the medium suitable for the culture of ES cells. Twenty-one days later, some colonies appeared that were morphologically different from the parental cancer cells (Fig. 1 *B* and *C*). Four weeks after transduction, we observed distinct types of colonies that were different from mock cells, transfected with pMXs retroviral vector as negative control (Fig. 1 *D* and *E*).

We examined the transfection and induction efficiencies by using combinations of *OCT3/4*, *SOX2*, *KLF4*, and *c-MYC*, and compared the results, with four cancer cell lines and human dermal fibroblasts (HDF) serving as controls (Fig. 1 *F–M*). In isolated colonies, we assessed *NANOG* promoter activity, which has been reported to be important in the acquisition of immature status (6–9), by co-transfection of *NANOG* promoter-*GFP* clone. *GFP* expression of transfectants was visualized by fluorescence microscopy (Fig. S2). From 1×10^4 cancer cells, we observed ≈10 *GFP*-expressing sphere formations. These cells in the present study were similar to iPS cells both in morphology, ES-like gene expression and epigenetic modifications as described in refs. 6–9, 13, and 14. Thus, we referred to these cells formed after transduction as iPC cells.

iPC Cells Express ES Cell Markers. Real-time RT-PCR using primers specific for retroviral transcripts confirmed efficient silencing of four retroviruses expressing *OCT3/4*, *SOX2*, *KLF4*, and *c-MYC* in iPC cells (Fig. 2*A*). RT-PCR showed that human iPC cells expressed undifferentiated ES cell-marker genes, including *NANOG*, *OCT3/4*, *SOX2*, *KLF4*, and *c-MYC*, although *NANOG* was not introduced exogenously (Fig. 2*B*). iPC cells expressed ES cell-specific surface antigens (15) including Ssea-4, tumor-related antigen (Tra)-1-60, Tra-1-81, and Tra-2-49 (Fig. 2 *C–G*) compared to the negative control (Fig. 2*H*).

In Vitro Differentiation of iPC Cells. To determine the differentiation ability of iPC cells, we used floating cultivation as embryoid bodies (EBs). Because iPC cells formed ball-shaped structures in suspension culture, we transferred these EB-like structures to EB culture conditions (EBC). These conditions were gelatin-coated plates maintained in DMEM/F12 containing 20% knockout-certified serum replacement. Culture was continued for another 7 days (Fig. 3*A*). Attached cells, named PostiPC cells, began to proliferate after 48 h. PostiPC cells were analyzed by the experiments described below and were compared to parental and iPC cells.

To determine the differentiation ability of iPC cells in vitro, we introduced iPC cells according to the methods of iPS (7). PostiPC cells showed various types of morphology, resembling those of epithelial cells, mesenchymal cells, and neuronal cells (Fig. 3 *B–E*). Immunocytochemistry detected cells that were positive for keratin 19 (Krt19) representing endoderm, vimentin (Vim) representing mesoderm and parietal endoderm, bIII-tubulin (Tubb3) representing ectoderm, and glial fibrillary acidic protein (Gfap) representing ectoderm (Fig. 3 *F–I*). RT-PCR confirmed, in addition to *VIM*, the expression of *FABP4* representing mesoderm, microtubule-associated protein 2 (*MAP2*) representing ectoderm, and paired box 6 (*PAX6*) representing ectoderm in PostiPC cells (Fig. 3*J*). The expression of *CDH1* representing endoderm and *KRT19* decreased in PostiPC cells. In particular, the gene expression of mesoderm and endoderm was increased in PostiPC cells, which was low or difficult to detect in the parental cells.

We then examined whether lineage-directed differentiation of iPC cells could be induced by methods reported for mesenchymal stem cells. We seeded iPC cells with supplements

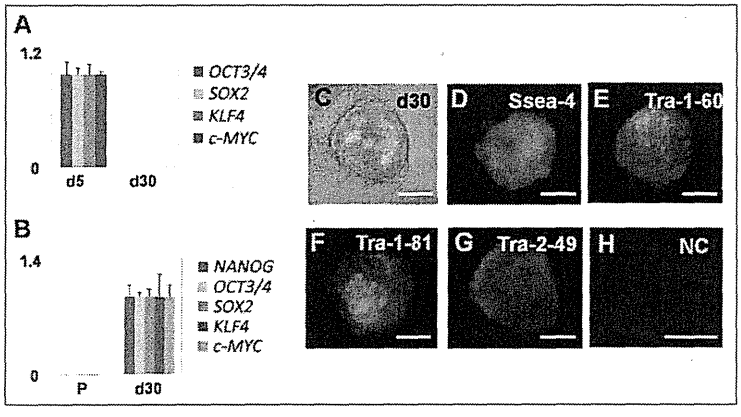

Fig. 2. iPC cells induced from DLD-1 expressing ES cell markers. (*A*) Real-time RT-PCR using primers specific for retroviral transcripts confirmed efficient silencing of four retroviruses expressing *OCT3/4*, *SOX2*, *KLF4*, and *c-MYC*. The mean value of d5 was set to 1 in each transcript. (*B*) iPC cells expressed undifferentiated ES cell-marker genes, including *NANOG*, *OCT3/4*, *SOX2*, *KLF4*, and *c-MYC*. The mean value of d30 was set to 1 in each transcript. (*C–G*) iPC cells were analyzed for several surface antigens, phase contrast (*C*), Ssea-4 (*D*), Tra-1-60 (*E*), Tra-1-81 (*F*), Tra-2-49 (*G*) and negative control (H). P, parental cells; NC, negative control. Scale bar: 200 μm. (Original magnification, ×200)

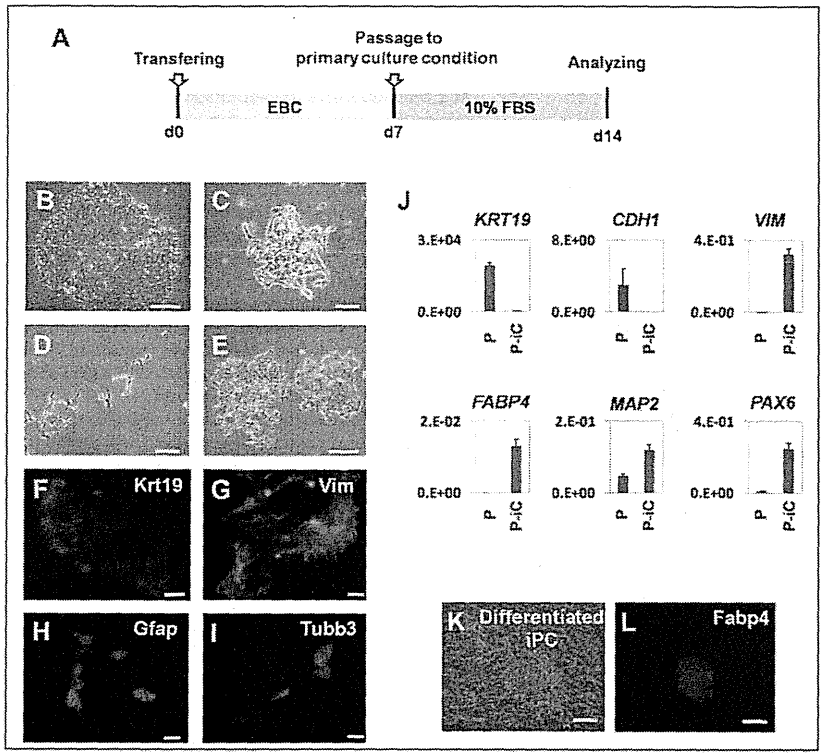

Fig. 3. Embryoid body (EB)-like formation mediated differentiation of iPC cells induced from DLD-1. (*A*) Schedule of induction from iPC cells to PostiPC cells. (*B–E*) After forming EB-like structures, iPC cells were transferred to primary culture conditions. Seven days later, attached (PostiPC) cells showed various morphologies, resembling those of epithelial cells (*B*), mesenchymal cells (*C*), neuronal cells (*D*), and mixed (*E*). (*F–I*) Immunocytochemistry confirmed the expression of Krt19 (*F*), Vim (*G*), Gfap (*H*), and Tubb3 (*I*) in these cells. (*J*) Real-time RT-PCR analysis verified the expression of differentiation markers, such as *KRT19, CDH1, VIM, FABP4, MAP2,* and *PAX6.* The expression of mRNA copies was normalized against *GAPDH* mRNA expression. (*K* and *L*) Directed differentiation of iPC cells into adipocytes showed differentiated iPC cells (*K*) that were positive for Fabp4 (*L*). P, parental cells; P-iC, PostiPC cells.

inducing adipocytes and maintained them under differentiation conditions for 2 weeks. The cells proliferated and immunocytochemistry detected cells positive for Fabp4 (Fig. 3 *K* and *L*). In contrast, immunocytochemistry on parental cells in the corresponding culture detected cells that were negative for Fabp4. These data demonstrated the possibility that iPC cells, compared to parental cells, could differentiate into three germ layers in vitro and indicated that cells acquired different properties.

Epigenetic Modification of Immature Status-Related Genes. Bisulfite genomic sequencing analyses were used to evaluate the methylation statuses of cytosine guanine dinucleotides (CpG) in the promoter regions of pluripotent-associated genes such as *NANOG*. The results revealed that the CpG dinucleotides of *NANOG* promoter were less methylated in transfected HDF (T-HDF) cells and two iPC clones, whereas the nucleotides were methylated in HDF, parental cancer cells, and PostiPC cells (Fig. 4*A*). Chromatin immunoprecipitation with trimethyl-histone H3 protein at lysine 4 (H3K4) antibody was used to analyze histone modification (Fig. 4*B*). The histone modification analyses for *NANOG* gene promoter showed that H3K4 was trimethylated in iPC, PostiPC, and T-HDF (14), whereas that of parental cancer cells and HDF was not detected. Similarly, the H3K4 trimethylation of *OCT3/4* gene promoter increased in iPC, PostiPC, and T-HDF, compared to parental cancer cells and HDF, respectively. The trimethylation of *SOX2* gene promoter was detected before and after the reprogramming of cancer cells, whereas the trimethylation of T-HDF, but not HDF, was detected. The trimethylation of *PAX6* and *MSX2* gene promoter was not detected. These findings demonstrated activation of the promoter regions of immature status-related genes in iPC cells.

Gene Expression and iPC and PostiPC Surface Markers. PostiPC cells, but not iPC cells, showed increased expression of several differentiation markers such as *FABP4, MAP2,* and *PAX6* (Fig. 3*J*), and markedly decreased expression of *NANOG, REX1, OCT3/4, SOX2, KLF4,* and *c-MYC*, which corresponded to those of parental cells (Fig. 5*A*). The expression of *P16(INK4A)* in PostiPC cells increased more than that in parental cells.

In colorectal cancer, the surface markers for CD24 and CD44 have been reported as CSC markers (16, 17). Flow cytometry showed that CD44 expression was markedly reduced in iPC cells and was increased in PostiPC cells. The CD44 expression level was relatively low in PostiPC cells compared with that of parental cells (Fig. 5*B*). CD 24 expression level was not changed apparently. The results showed the transition of the population from parental cells to PostiPC, suggesting an alteration of biological characteristics, such as sensitivity to chemicals.

Sensitivity of Anticancer Drug and Differentiation-Inducing Chemicals. The methyl thiazolyl tetrazolium (MTT) assay showed that PostiPC cells acquired sensitivity to 5-fluorodeoxyuridine (5-FU) to a greater degree than parental cells ($n = 11$, $P = 0.003$, Wilcoxon rank test; Fig. 6*A*). These data suggest the possibility that PostiPC cells, via iPC cells, could be more sensitive to therapeutic agents.

Proliferation assays for 48 h in Matrigel and the mTeSR1 medium, an ES-culture condition, showed that iPC cell growth significantly decreased compared with parental cells based on mean cell counts in four independent wells ($n = 4$, $P = 0.046$, Wilcoxon rank test; Fig. 6*B*). There was, however, no significant difference in 48-h proliferation of parental and PostiPC cells in primary culture conditions (Fig. 6*C*). An invasion assay showed no significant differences between parental and PostiPC cells (Fig. 6*D*). In a sharp contrast, the 48-h proliferation assays with the presence of retinoic acid (RA) and 1,25-dihydroxy vitamin D3 (VD3), which are known as inducers of differentiation (18, 19), resulted in a reduction in PostiPC cells compared with mock-treated parental cells ($n = 8$, $P = 0.512$ and 0.049, respectively, Wilcoxon rank test; Fig. 6 *E* and *F*). Invasion assays were performed after the 48-h treatment; the data indicated that, in the presence of RA and VD3, the invasion activity of PostiPC cells was reduced compared with parental cells ($n = 6$, $P = 0.013$ and 0.003, respectively, Wilcoxon rank test; Fig. 6 *G* and *H*).

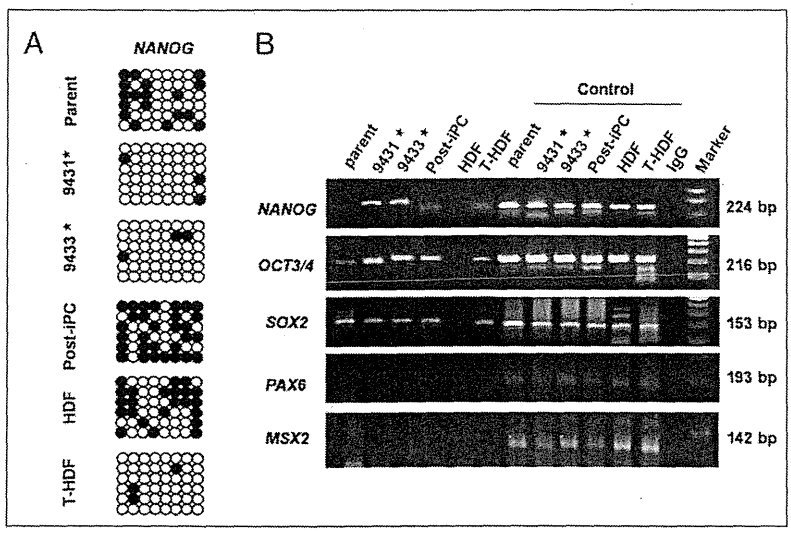

Fig. 4. Epigenetic modification of immature status-related genes evaluated with bisulfite sequencing analysis and chromatin immunoprecipitation in DLD-1. (*A*) From the analysis of epigenetic status, bisulfite genomic sequencing analyses in the promoter regions of genes inducing immature status, *NANOG*, revealed that they were not methylated appreciably in iPC cells (clones 9431 and 9433), whereas the CpG dinucleotides of the regions were methylated in parental cancer cells and PostiPC cells (open and closed circles indicate unmethylated and methylated, respectively). (*B*) Chromatin immunoprecipitation with trimethyl-K4 H3 antibody was used to analyze the histone modification status in parental, iPC, and PostiPC cells. H3 lysine 4 was methylated in these regions for *NANOG* in iPC cells compared to that in parental and PostiPC cells. H3 lysine 4 was methylated in these regions for *OCT3/4* in iPC and PostiPC cells compared to those in parental cells (results were assessed in contrast to each input DNA). HDF and transfected HDF (T-HDF) were analyzed for comparison. As a control, respective sheared chromatin sample was used for quantitative PCR. *, clones of iPC cells.

Assessment of Tumorigenic Properties. To determine tumorigenic properties in vivo, PostiPC cells were transplanted s.c. at several densities into dorsal flanks of NOD/SCID mice. Four weeks after injection, we observed tumor formation (Fig. S3*A*). There were significant differences between PostiPC cells and parental cells ($P < 0.01$, Wilcoxon rank test; Fig. S3*B*). These data demonstrated the reduction of tumorigenesis via reprogramming process; this finding may be applied to anticancer therapy.

Discussion

The role of CSCs was noted in acute myeloid leukemia (3). The possible involvement of CSCs has since been shown in several solid tumors (20–22). In solid tumors, these results suggest that the CSC population, although it is likely a minority, is related to treatment resistance and problems of relapse or metastasis (1, 2). CSCs, through their self-renewal and drug-resistant capacities, may share properties that are conducive to persistence and proliferation, even after anticancer therapy. It is important to understand their biological characteristics, as specific markers of all CSCs have not yet been identified.

Recently, several reports have shown that tumor development is associated with genetic and epigenetic changes of the genome, and that epigenetic modifications play an important role in tumor heterogeneity (23). Several experiments, such as nuclear transplantation, ES cell fusion, and transfection with several transcription factors, have demonstrated reprogramming of terminally differentiated cells into pluripotent embryonic cells, which is linked to the development of an organism by resetting the epigenetic modifications (4–9). In previous reports, the transcription factor *NANOG* was required to maintain the pluripotency and self-renewal of ES cells (13, 14).

According to genetic and epigenetic analyses in previous reports, immature status related to promoter activation in defined genes, such as *NANOG*, plays a very important role in the establishment of a pluripotent state (6–9, 13, 14). To prepare iPC cells, we manufactured a specific tool that could detect the pluripotent

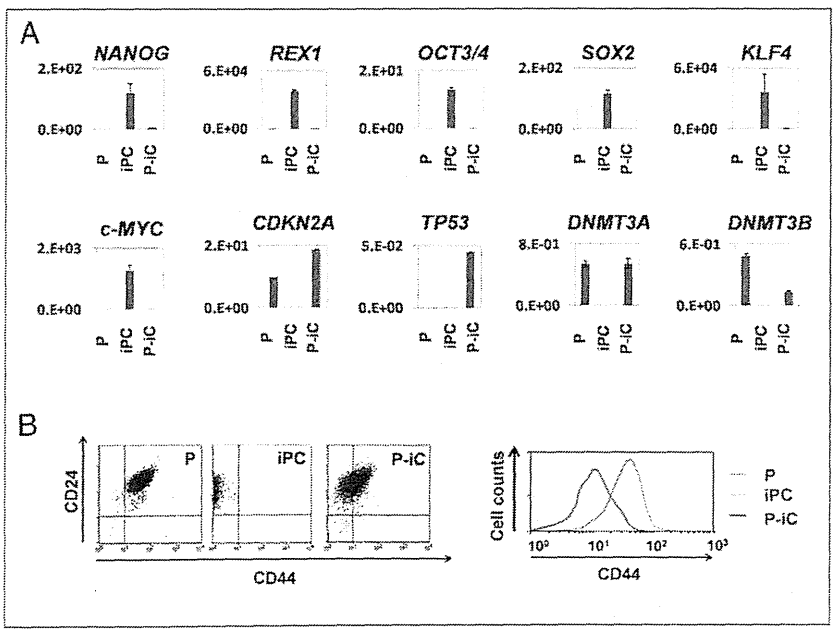

Fig. 5. Expression of immature and differentiated status-related genes in parental, iPC, and PostiPC cells induced from DLD-1. (*A*) The expression of *NANOG*, *REX1*, *OCT3/4*, *SOX2*, *KLF4*, and *c-MYC* markedly decreased in iPC cells. The expression of *CDKN2A*, *DNMT3A*, and *DNMT3B* increased in PostiPC cells compared to iPC cells. The mRNA copy expression was normalized against *GAPDH* mRNA expression. (*B*) (*Left*) Flow cytometry showed a shift of the CD24/CD44 population in parental, iPC, and PostiPC cells. (*Right*) The CD44 population in PostiPC cells decreased compared with that of parental cells. P, parental cells; P-iC, PostiPC cells.

CELL BIOLOGY

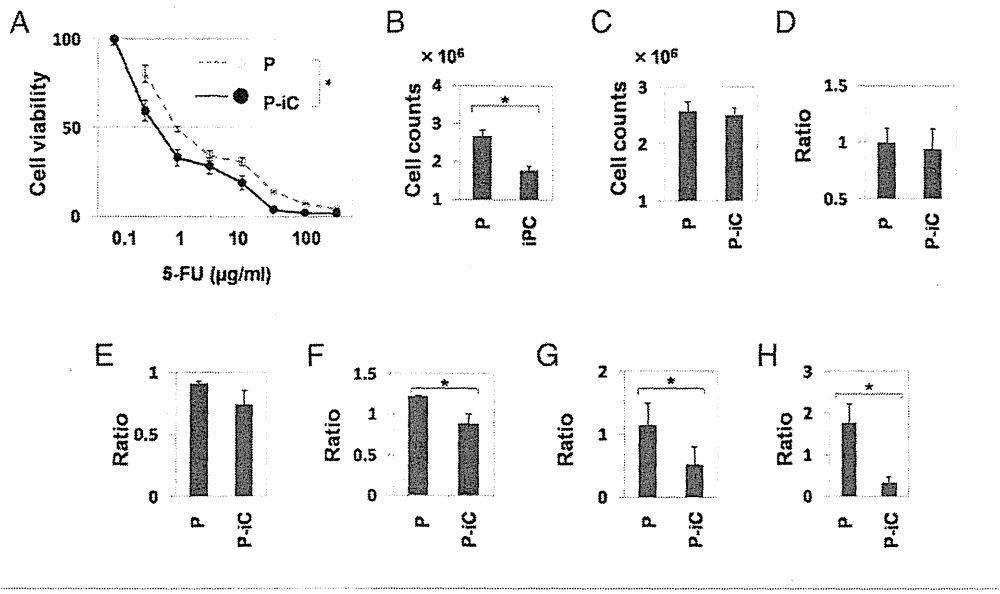

Fig. 6. In vitro methyl thiazolyl tetrazolium (MTT) analyses, proliferation and invasion assay. (*A*) The 5-FU MTT assay revealed significant differences in PostiPC and DLD-1 parental cells ($n = 11$, $P = 0.003$, Wilcoxon rank test). (*B*) Proliferation assays for ES-culture conditions showed differences in growth of iPC cells and DLD-1 parental cells ($n = 4$, $P = 0.046$, Wilcoxon rank test). (*C*) Proliferation assays in primary culture conditions showed no significant differences between DLD-1 parental and PostiPC cells. (*D*) Invasion assay showed no significant differences between DLD-1 parental and PostiPC cells (relative ratio and parental cell average). (*E* and *F*) Proliferation assays showed differences in ratio with control (with no treatment) under the differentiation-inducing treatment with vitamins A and D supplementation ($n = 8$, $P = 0.512$ and 0.049, respectively, Wilcoxon rank test). (*G* and *H*) Invasion assays showed significant differences in the ratio with control (with no treatment) cells under the differentiation-inducing treatment with vitamin A and D supplementation ($n = 6$, $P = 0.013$ and 0.003, respectively, Wilcoxon rank test). P, parental cells; P-iC, PostiPC cells. *, $P < 0.05$.

state in living cells based on the results of previous studies. We investigated *NANOG* expression in gastrointestinal cancer cell lines, corresponding to human iPS cells and teratocarcinoma NTERA-2, which had higher *NANOG* expression. The expression could not be detected in PostiPC cells with this system. A low efficiency, as shown in iPS (6–9, 13, 14), suggests a possibility that only a minority of tumor cell lines possesses specific potential to obtain the property of iPC, or more likely that multiple mechanisms are involved in full execution of reprogramming. We have to consider a possibility that sphere-forming cells might be rare among the original cancer cell populations.

In this study, the tumor-suppressor gene *P16(INK4A)*, which acts against the self-renewal of ES cells (10, 12), was repressed in iPC cells. Our analysis indicated that *P16(INK4A)* expression increased in PostiPC cells, which may relate to the notion that *P16(INK4A)* up-regulation is involved in the suppression of transformed phenotypes and their sensitization to therapeutic agents (24). The sequence study of *P16(INK4A)* promoter indicated the demethylation in PostiPC cells from DLD-1 cells, whereas the sequence of parental cells was methylated. This study suggests that the reactivation of tumor suppressor genes by reprogramming may play a role in increased chemosensitivity to 5-FU and the regression of cell proliferation and invasiveness under differentiation-inducing conditions. The *Rb/P16(INK4A)* tumor-suppressive pathway has been reported to be abrogated in several tumors (24). It is necessary to investigate the specific analysis in the pathways to assess the contribution of TSG.

Presumably, the suppression of tumors and their sensitization to induced differentiation are the result of genetic and epigenetic modifications. This result supports the possibility of new cancer therapies via reprogramming approaches even in cancer cells that should have corrupted genetic codes. In the present study, iPC cells were induced from eight cancer cells, including cancers of colorectum, esophagus, stomach, pancreas, liver and bile ducts (Fig. S4). Here, iPC was established from cancer cell lines. It is necessary to demonstrate universality in primary tumors and to more efficiently investigate the factors and population in relation to the induction of iPC cells: points to be elucidated and developed include differences of normal and tumor cells, individual responses, efficiency, and reagent delivery system. As novel therapeutic approaches, the heterogeneity of reprogrammed cancer cells remains to be investigated.

Materials and Methods

Cell Lines and Culture. Twenty cell lines derived from human gastrointestinal cancers included colorectal cancer (Caco2, DLD-1, HCT116, HT-29, KM12SM, LoVo, and SW480), esophageal cancer (TE-10), gastric cancer (MKN45), pancreatic cancer (BXPC-3, MIAPaCa-2, PANC-1, and PSN-1), hepatocellular carcinoma (Hep3B, HepG2, HLE, HLF, HuH-7, and PLC), cholangiocellular carcinoma (HuCCT-1), and teratocarcinoma (NTERA-2 clone D1). NTERA-2 was provided by DS Pharma Biomedical (Osaka). These cell lines were maintained in DMEM (Nakalai Tesque, Kyoto) containing 10% FBS at 37 °C under a 5% humidified CO_2 atmosphere. HDF was purchased from Toyobo (CA106K05a; Osaka) as a normal cell control and maintained with the Fibroblast Growth Medium kit (CA116500; Toyobo). Plasmids were purchased from Addgene (Cambridge, MA), Clontech (Palo Alto, CA), Cell Biolabs (San Diego), and Open Biosystems (Huntsville, AL). The plasmids used in this study are summarized in Table S1. These transfectants were grown in DMEM supplemented with 10% FBS and puromycin (2 μg/mL), and transferred to specific culture conditions as described in the supporting information. All transfectants with retrovirus were made with the ViraDuctin retrovirus transduction kit (Cell Biolabs). Those with lentivirus were made with the Virapower packaging mix (Invitrogen, Carlsbad, CA) or Arrest-In (Open Biosystems). In brief, cancer cell lines were transfected with adequate plasmid at a concentration of 4 μg/μl by using lipofectamine (Lipofectamine 2000; Invitrogen), and incubated in glucose-free Opti-MEM (Invitrogen). All experiments were performed at 50–70% cell confluence and results were confirmed in at least three independent experiments. All-in-one-type fluorescence microscopy

(BZ-8000; Keyence, Osaka) with digital photographic capability was used to visualize cells at several magnifications. The growth rates of the cultured gastrointestinal cancer cell lines were measured by counting cells using CellTac (Nihon Koden, Tokyo). The optimization of retroviral transduction of human cancer cell lines was performed as shown in supporting information. Vectors used are shown in Table S1.

RNA Preparation and RT-PCR. Total RNA was prepared by using TRIzol reagent (Invitrogen). Reverse transcription was performed with SuperScriptIII (Invitrogen). To confirm PCR amplification, 25–35 cycles of the PCR were performed by using a PCR kit (Takara, Kyoto) on a Geneamp PCR system 9600 (PE Applied Biosystems, Foster City, CA) with the following condition: 95 °C for 10 s, 60 °C for 10 s, and 72 °C for 60 s. An 8-μl aliquot of each reaction mixture was size-fractionated in a 1.5% agarose gel and visualized with ethidium bromide staining. To confirm RNA quality, PCR amplification was performed for the glyceraldehyde-3-phosphate dehydrogenase (*GAPDH*) gene using the specific primers (Tables S2 and S3). For quantitative assessment, we evaluated the gene expression by RT-PCR analysis. Quantitative real-time RT-PCR was performed by using a LightCycler TaqMan Master kit (Roche Diagnostics, Tokyo) for cDNA amplification of target specific genes. The expression of mRNA copies was normalized against *GAPDH* mRNA expression. The detailed condition for Quantitative real-time RT-PCR assessment is shown in supporting information. Primers used are shown in Tables S2 and S3.

Drugs and Antibodies. Antibodies used for immunocytology were against Nanog, Ssea-3, Ssea-4, Tra-1-60, Tra-1-81, Tra-2-49, Tubb3, Gfap, Vim (Chemicon International, Temecula, CA), and Krt19 (OriGene Technologies, Rockville, MD). Differentiation to adipocytes was induced by specific supplements (Adipogenic Supplement 390416; Invitrogen).

Bisulfite Sequencing. Genomic DNA was treated with Applied Biosystems methySEQr Bisulfite Conversion kit (Applied Biosystems) according to the manufacturer's recommendations. Treated DNA was purified with QIAquick column (Qiagen, Valencia, CA). The human *NANOG* gene promoter regions were amplified by PCR. The PCR products were subcloned with pCR2.1-TOPO. Every clone of each sample was verified by sequencing with the T3 and T7 primers. The analysis used Sequencing Analysis Software v5.2 (Applied Biosystems). Primer sequences used for PCR amplification are provided in Table S3.

Chromatin Immunoprecipitation Assay. Approximately 1×10^7 cells were cross-linked with 1% formaldehyde for 10 min at room temperature and quenched by adding glycine. The cell lysate was treated to share a chromatin-DNA complex with an enzymatic shearing kit (Active Motif, Carlsbad, CA). Immunoprecipitation used Protein G magnetic beads (Active Motif)-linked anti-trimethyl lysine 4 histone H3 antibody (Nippongene, Toyama, Japan), or a negative control IgG kit (Active Motif). Eluates were used as templates for quantitative PCR. Each sheared chromatin sample was used for quantitative PCR as a control. Primer sequences used for PCR amplification are provided in Table S3.

Flow Cytometry. Flow cytometry was performed on trypsin-dissociated parental cells, iPC, and PostiPC cells by using antibodies for CD24 (BD Biosciences, Sparks, MD) and CD44 (BD Biosciences). 7-AAD (eBioscience, San Diego, CA) preincubation was used to exclude dead cells. To assess the expression of the reprogrammed cells, iPC cells were assessed in the isolated colonies after the transfection of *NANOG* promoter-*GFP* clone. Cells were analyzed by using a FACScan flow cytometer equipped with CellQuest software (FACS caliber; BD Biosciences).

RA and VD3 Treatment. RA and VD3 were purchased from Sigma–Aldrich (St. Louis). RA was dissolved in 99% ethanol as a 100 μM stock solution. The cells were allowed to settle for 48 h in DMEM supplemented with 100 nM RA. VD3 was dissolved in 99% ethanol as a 10 M stock solution. The cells were allowed to settle for 48 h in DMEM supplemented with 10 nM VD3. To assess the proliferation in the presence of RA and VD3, the cells were grown in these media for another 48 h. Cell viability was determined with the Cell Counting kit incorporating WST-8 (Dojindo Lab., Tokyo). WST-8 (10 μL) was added to 100 μL of the medium containing each supplement above, and the absorbance was read at 450 nm by using a microplate reader (Model 680XR; Bio-Rad Laboratories, Hercules). All experiments were performed at 30–80% cell confluence, and the results were confirmed in at least three independent experiments.

Chemosensitivity Assessment. To assess the sensitivity to 5-FU in vitro, cells at different concentrations were evaluated with an MTT assay. 5-FU was purchased from Kyowa Hakkou (Tokyo). The cells were allowed to settle for 96 h in DMEM supplemented with several concentrations of 5-FU, and viability was assessed.

Invasion Assays. Cell invasion was assessed with a CytoSelect Cell Invasion Assay according to the manufacturer's protocol (Cell Biolabs). Cells (1.0×10^5) in DMEM were placed on 8.0-m-pore size membrane inserts in 96-well plates, and DMEM with 10% FBS was placed in the bottom of the wells. After 24 h, cells that did not invade were removed from the top side of the membrane chamber, and the cells from the underside of the membrane were completely dislodged by tilting the membrane chamber in Cell Detachment Solution (Cell Biolabs). Lysis Buffer/CyQuannt GR dye solution (Cell Biolabs) was added to each well, and the fluorescence of the mixture was read with a fluorescence plate reader at 480 nm/520 nm.

In Vivo Analysis. The tumorigenic properties were evaluated on trypsin-dissociated cells with parental and PostiPC cells. We transplanted them suspended in DMEM/Matrigel (BD Biosciences) s.c. into the dorsal flanks of NOD/SCID mice (CREA, Tokyo) in several concentrations. Tumors were dissected and measured 4 weeks after injection.

Statistical Analysis. For continuous variables, the results are expressed as means ± SEs of the mean. The relationships among gene expressions or cell counts were analyzed with χ^2 and Wilcoxon rank tests. All tests were analyzed with JMP software (SAS Institute, Cary, NC). Differences with P values <0.05 were considered statistically significant.

1. Reya T, Morrison SJ, Clarke MF, Weissman IL (2001) Stem cells, cancer, and cancer stem cells. *Nature* 414:105–111.
2. Pardal R, Clarke MF, Morrison SJ (2003) Applying the principles of stem-cell biology to cancer. *Nat Rev Cancer* 3:895–902.
3. Bonnet D, Dick JE (1997) Human acute myeloid leukemia is organized as a hierarchy that originates from a primitive hematopoietic cell. *Nat Med* 3:730–737.
4. Thomson JA, et al. (1998) Embryonic stem cell lines derived from human blastocysts. *Science* 282:1145–1147.
5. Hochedlinger K, Jaenisch R (2006) Nuclear reprogramming and pluripotency. *Nature* 441:1061–1067.
6. Takahashi K, Yamanaka S (2006) Induction of pluripotent stem cells from mouse embryonic and adult fibroblast cultures by defined factors. *Cell* 126:663–676.
7. Takahashi K, et al. (2007) Induction of pluripotent stem cells from adult human fibroblasts by defined factors. *Cell* 131:861–872.
8. Yu J, et al. (2007) Induced pluripotent stem cell lines derived from human somatic cells. *Science* 318:1917–1920.
9. Yu J, et al. (2009) Human induced pluripotent stem cells free of vector and transgene sequences. *Science* 324:797–801.
10. Dabelsteen S, et al. (2009) Epithelial cells derived from human embryonic stem cells display p16INK4A senescence, hypermotility, and differentiation properties shared by many P63+ somatic cell types. *Stem Cells* 27:1388–1399.
11. Hong H, et al. (2009) Suppression of induced pluripotent stem cell generation by the p53-p21 pathway. *Nature* 460:1132–1135.
12. Li H, et al. (2009) The Ink4/Arf locus is a barrier for iPS cell reprogramming. *Nature* 460:1136–1139.
13. Loh YH, et al. (2006) The Oct4 and Nanog transcription network regulates pluripotency in mouse embryonic stem cells. *Nat Genet* 38:431–440.
14. Wu Q, et al. (2006) Sall4 interacts with Nanog and co-occupies Nanog genomic sites in embryonic stem cells. *J Biol Chem* 281:24090–24094.
15. Adewumi O, et al.;International Stem Cell Initiative (2007) Characterization of human embryonic stem cell lines by the International Stem Cell Initiative. *Nat Biotechnol* 25: 803–816.
16. Vermeulen L, et al. (2008) Single-cell cloning of colon cancer stem cells reveals a multi-lineage differentiation capacity. *Proc Natl Acad Sci USA* 105:13427–13432.
17. Du L, et al. (2008) CD44 is of functional importance for colorectal cancer stem cells. *Clin Cancer Res* 14:6751–6760.
18. Huang ME, et al. (1988) Use of all-trans retinoic acid in the treatment of acute promyelocytic leukemia. *Blood* 72:567–572.
19. zur Nieden NI, Kempka G, Ahr HJ (2003) In vitro differentiation of embryonic stem cells into mineralized osteoblasts. *Differentiation* 71:18–27.
20. Singh SK, et al. (2004) Identification of human brain tumour initiating cells. *Nature* 432:396–401.
21. Kim CF, et al. (2005) Identification of bronchioalveolar stem cells in normal lung and lung cancer. *Cell* 121:823–835.
22. O'Brien CA, Pollett A, Gallinger S, Dick JE (2007) A human colon cancer cell capable of initiating tumour growth in immunodeficient mice. *Nature* 445:106–110.
23. Hahn WC, Weinberg RA (2002) Rules for making human tumor cells. *N Engl J Med* 347:1593–1603.
24. Sherr CJ, McCormick F (2002) The RB and p53 pathways in cancer. *Cancer Cell* 2: 103–112.

20111800 1B (3/3)

厚生労働科学研究費補助金

第3次対がん総合戦略研究事業

幹細胞制御によるがん治療法開発のための基盤研究

平成21-23年度　　**総合・分担研究報告書**

研究代表者　落谷　孝広

平成24（2011）年5月

（3／3冊）

Published in final edited form as:
Gastroenterology. 2009 March ; 136(3): 1012–1024. doi:10.1053/j.gastro.2008.12.004.

EpCAM-positive hepatocellular carcinoma cells are tumor initiating cells with stem/progenitor cell features

Taro Yamashita[1], **Junfang Ji**[1], **Anuradha Budhu**[1], **Marshonna Forgues**[1], **Wen Yang**[2], **Hong-Yang Wang**[2], **Huliang Jia**[3], **Qinghai Ye**[3], **Lun-Xiu Qin**[3], **Elaine Wauthier**[4], **Lola M. Reid**[4], **Hiroshi Minato**[5], **Masao Honda**[5], **Shuichi Kaneko**[5], **Zhao-You Tang**[3], and **Xin Wei Wang**[1,a]

[1]Liver Carcinogenesis Section, Laboratory of Human Carcinogenesis, Center for Cancer Research, National Cancer Institute, Bethesda, MD 20892-4258, USA

[2]International Cooperation Laboratory on Signal Transduction, Eastern Hepatobiliary Surgery Institute, Shanghai 200438, China

[3]Liver Cancer Institute and Zhongshan Hospital, Fudan University, Shanghai 200032, China;

[4]Department of Cell and Molecular Physiology, University of North Carolina School of Medicine, Chapel Hill, NC 27599, USA

[5]Liver Disease Center and Kanazawa University Hospital, Kanazawa University, Kanazawa, 920-8641, Japan.

Abstract

Background & Aims—Cancer progression/metastases and embryonic development share many properties including cellular plasticity, dynamic cell motility, and integral interaction with the microenvironment. We hypothesized that the heterogeneous nature of hepatocellular carcinoma (HCC) may be, in part, due to the presence of hepatic cancer cells with stem/progenitor features.

Methods—Gene expression profiling and immunohistochemistry analyses were used to analyze 235 tumor specimens derived from two recently identified HCC subtypes ($EpCAM^+$ AFP^+ HCC and $EpCAM^-$ AFP^- HCC). These subtypes differed in their expression of alpha-fetoprotein (AFP), a molecule produced in the developing embryo, and EpCAM, a cell surface hepatic stem cell marker. Fluorescence-activated cell sorting (FACS) was used to isolate $EpCAM^+$ HCC cells, which were tested for hepatic stem/progenitor cell properties.

Results—Gene expression and pathway analyses revealed that the $EpCAM^+$ AFP^+ HCC subtype had features of hepatic stem/progenitor cells. Indeed, the FACS-isolated $EpCAM^+$ HCC cells displayed hepatic cancer stem cell-like traits including the abilities to self-renew and differentiate. Moreover, these cells were capable of initiating highly invasive HCC in NOD/SCID mice. Activation of Wnt/β-catenin signaling enriched the $EpCAM^+$ cell population, while RNA interference-based blockage of EpCAM, a Wnt/β-catenin signaling target, attenuated the activities of these cells.

Conclusions—Taken together, our results suggest that HCC growth and invasiveness is dictated by a subset of $EpCAM^+$ cells, opening a new avenue for HCC cancer cell eradication by targeting Wnt/β-catenin signaling components such as EpCAM.

aCorrespondence: Liver Carcinogenesis Section, LHC, CCR, NCI, 37 Convent Drive, Building 37, Room 3044A, MSC 4258, Bethesda, MD 20892-4258, USA; Phone: 301-496-2099; Fax: 301-496-0497; xw3u@nih.gov..

Disclosures: No conflicts of interest exist.

Microarray data: Publicly available at http://www.ncbi.nlm.nih.gov/geo/ (Accession number: GSE5975).

INTRODUCTION

Tumors originate from normal cells as a result of accumulated genetic/epigenetic changes. Although considered monoclonal in origin, tumor cells are heterogeneous in their morphology, clinical behavior, and molecular profiles [1, 2]. Tumor cell heterogeneity has previously been explained by the clonal evolution model [3], however, recent evidence has suggested that heterogeneity may be due to derivation from endogenous stem/progenitor cells [4] or de-differentiation of a transformed cell 5. This hypothesis supports an early proposal that cancers represent "blocked ontogeny" 6 and a derivative that cancers are transformed stem cells 7. This renaissance of stem cells as targets of malignant transformation has led to realizations about the similarities between cancer cells and normal stem cells in their capacity to self-renew, produce heterogeneous progenies, and limitlessly divide [8]. The cancer stem cell (CSC) (or Tumor Initiating Cell) concept is that a subset of cancer cells bears stem cell features that are indispensable for a tumor. Accumulating evidence suggests the involvement of CSCs in the perpetuation of various cancers including leukemia, breast cancer, brain cancer, prostate cancer and colon cancer [9-13]. Experimentally, putative CSCs have been isolated using cell surface markers specific for normal stem cells. Stem cell-like features of CSC have been confirmed by functional *in vitro* clonogenicity and *in vivo* tumorigenicity assays. For example, leukemia-initiating cells in NOD/SCID mice are $CD34^{++}CD38^{-}$ [11]. Breast cancer CSCs are $CD44^{+}CD24^{-/low}$ cells while tumor initiating cells of the brain, colon and prostate are $CD133^{+}$ [10, 12, 13]. CSCs are considered more metastatic and drug/radiation resistant than non-CSCs in the tumor, and are responsible for cancer relapse. These findings warrant the development of treatment strategies that can specifically eradicate CSCs [14, 15].

Hepatocellular carcinoma (HCC) is the third leading cause of cancer death worldwide [16]. Although the cellular origin of HCC is unclear [17, 18], HCC has heterogeneous pathologies and genetic/genomic profiles 19, suggesting that HCC can initiate in different cell lineages 20. The liver is considered as a maturational lineage system similar to that in the bone marrow [21]. Experimental evidence indicates that certain forms of hepatic stem cells (HpSC), present in human livers of all donor ages, are multipotent and can give rise to hepatoblasts (HB) [22, 23], which are, in turn, bipotent progenitor cells that can progress either into the hepatocytic or biliary lineages [22, 24]. Alpha-fetoprotein (AFP) is one of the earliest markers detected in the liver bud specified from the ventral foregut [25, 26], but its expression has only been found in HB and to a lesser extent in committed hepatocytic progenitors, not in later lineages nor in normal human HpSC 22. Recent studies also indicate that EpCAM is a biomarker for HpSC as it is expressed in HpSCs and HBs [22-24].

We recently identified a novel HCC classification system based on EpCAM and AFP status [27]. Gene expression profiles revealed that $EpCAM^{+}$ AFP^{+} HCC (referred to as Hepatic Stem Cell-like HCC; HpSC-HCC) has progenitor features with poor prognosis, whereas $EpCAM^{-}$ AFP^{-} HCC (referred to as Mature Hepatocyte-like HCC; MH-HCC) have adult hepatocyte features with good prognosis. Wnt/β-catenin signaling, a critical player for maintaining embryonic stem cells [28], is activated in $EpCAM^{+}$ AFP^{+} HCC, and EpCAM is a direct transcriptional target of Wnt/β-catenin signaling [29]. Moreover, $EpCAM^{+}$ AFP^{+} HCC cells are more sensitive to β-catenin inhibitors than $EpCAM^{-}$ HCC cells *in vitro* [29]. Interestingly, a heterogeneous expression of EpCAM and AFP was observed in clinical tissues, a feature that may be attributed to the presence of a subset of CSCs. In this study, we have confirmed that $EpCAM^{+}$ HCC cells are highly invasive and tumorigenic, and have activated Wnt/β-catenin signaling. We also demonstrate a crucial role of EpCAM in the maintenance of hepatic CSCs. Our data shed new light on the pathogenesis of HCC and may open new avenues for therapeutic interventions for targeting hepatic CSCs.

Materials and Methods

Clinical Specimens

HCC samples were obtained with informed consent from patients who underwent radical resection at the Liver Cancer Institute of Fudan University, Eastern Hepatobiliary Surgery Institute and the Liver Disease Center of Kanazawa University Hospital, and the study was approved by the Institutional Review Board of the respective Institutes. The microarray data from clinical specimens are publicly available (GEO accession number, GSE5975) [27]. Array data from a total of 156 HCC cases (155 hepatitis B virus-positive) corresponding to two subtypes of HCC, i.e., HpSC-HCC and MH-HCC, were used to search for HpSC-HCC-associated genes (Suppl Table 3). A total of 79 formalin fixed and paraffin-embedded HCC samples were used for IHC analyses (Suppl Table 4), 56 of which were also used in a recent study [30]. The classification of HpSC-HCC and MH-HCC were based on previously described criteria [27].

Cell Cultures and Sorting

Human liver cancer cell lines (HuH1 and HuH7) were derived from Health Science Research Resources Bank (JCRB0199 and JCRB0403, respectively) and routinely cultured as previously described 31. Normal human MHs, provided by the University of Pittsburgh through LTPADS, were cultured as previously described 32. Human HpSCs were isolated from fetal livers and cultured in Kubota's Medium as previously described 33. Wnt10B conditioned medium was prepared as described 34. Embryonic stem cell culture medium was prepared using Knockout™ DMEM supplemented with 18% of Serum Replacement (Invitrogen). The pTOP-FLASH and pFOP-FLASH luciferase constructs were previously described [29]. BIO and MeBIO were generous gifts from Ali Brivanlou (The Rockefeller University, New York, NY). For isolating single cell-derived colonies to determine whether heterogeneity is an intrinsic property of $EpCAM^+$ cells, HuH1 and HuH7 cells were resuspended and plated as a single cell per well in 96-well plates. A total of 192 single cells were successfully plated. The clones which grew well were selected two weeks after seeding and used for IF analysis. The 5FU stock (2 mg/ml; Sigma, St. Louis, MO), was prepared in distilled water. Fluorescence Activated Cell Sorting (FACS) and Magnetic Activated Cell Sorting (MACS) analyses were used to isolate $EpCAM^+$ HCC cells (supplemental materials).

Clonogenicity, spheroid formation, invasion, quantitative RT-PCR and immunohistochemistry (IHC) assays

For colony formation assays, 2,000 $EpCAM^+$ or $EpCAM^-$ cells were seeded in 6-well plates after FACS. After 10 days of culture, cells were fixed by 100% methanol and stained with methylene blue. For spheroid assays, single cell suspensions of 1,000 $EpCAM^+$ or $EpCAM^-$ cells were seeded in 6-well Ultra-Low Attachment Microplates (Corning, Corning, NY) after FACS. The number of spheroids was measured 14 days after seeding. Invasion assays were performed using BD BioCoat™ Matrigel Matrix Cell Culture Inserts and Control Inserts (BD Biosciences) essentially as previously described [31]. RT-PCR and IHC assays are described in details in the supplemental materials.

Tumorigenicity in NOD/SCID Mice

Six-week-old NOD/SCID mice (NOD/NCrCRl-*Prkdc*^{scid}) were purchased from Charles River (Charles River Laboratories, Inc., Wilmington, MA). The protocol was approved by the NCI-Bethesda Animal Care and Use Committee. Cells were suspended in 200 μl of DMEM and Matrigel (1:1), and subcutaneous injection was performed. The size and incidence of subcutaneous tumors were recorded. For histological evaluation, tumors were formalin-fixed

paraffin-embedded or directly embedded in O.C.T. compound (Sakura Finetek, Torrance, CA) and stored in −80°C.

RNA interference

A siRNA specific to *TACSTD1* (SI03019667) and a control siRNA (1022076) were designed and synthesized by Qiagen (Qiagen, Valencia, CA). Transfection was performed using Lipofectamine 2000 (Invitrogen), according to the manufacturer's instructions. A total of 200 nM of siRNA duplex was used for each transfection.

Statistical Analyses

The class comparison and gene clustering analyses were performed as previously described [30]. The canonical pathway analysis was performed using Ingenuity Pathways Analysis (v5.5, Ingenuity® Systems). The association of HCC subtypes and clinicopathological characteristics was examined using either Mann-Whitney U-tests or χ^2 tests. Student t-tests were used to compare various test groups assayed by colony formation, spheroid formation or invasion assays. The Kaplan-Meier survival analysis was performed to compare patient survival or tumorigenecity.

RESULTS

A poor prognostic HCC subtype with molecular features of HpSC

We re-evaluated the gene expression profiles that were uniquely associated with two recently identified prognostic subtypes of HCC, i.e., HpSC-HCC and MH-HCC, using a publicly available microarray dataset of 156 HCC cases (GEO accession number: GSE5975). Sixty cases were defined as HpSC-HCC with a poor prognosis while 96 cases were defined as MH-HCC with a good prognosis, based on EpCAM and AFP status [27]. A class comparison analysis with univariate t-tests and a global permutation test (x1000) yielded 793 genes that were differentially expressed between HpSC-HCC and MH-HCC ($P < 0.001$). Hierarchical cluster analyses revealed two main gene clusters that were upregulated (cluster-A; 455 genes) or downregulated (cluster-B; 338 genes) in HpSC-HCC (Fig 1A). Pathway analysis indicated that the enriched genes in cluster-A were significantly associated with known stem cell signaling pathways such as TGF-β, Wnt/β-catenin, PI3K/Akt and integrin ($P < 0.01$) (Fig 1B). In contrast, genes in cluster-B were significantly associated with mature hepatocyte functions such as xenobiotic metabolism, complement system, and coagulation system ($P < 0.01$). Noticeably, known HpSC markers such as *KRT19* (CK19), *TACSTD1* (EpCAM), *AFP, DKK1, DLK1* and *PROM1* (CD133) were significantly upregulated in HpSC-HCC while known liver maturation markers such as *UGT2B7* and *CYP3A4* were more abundantly expressed in MH-HCC (Fig 1C) (Suppl Tables 1-2). Kaplan-Meier survival analysis revealed that HpSC-HCC patients had a significantly shorter survival than MH-HCC patients ($P = 0.036$) (Fig 1D). Consistently, HpSC-HCC patients had a high frequency of macroscopic and microscopic portal vein invasion (Fig 1E).

However, IHC analyses of an additional 79 HCC cases revealed that among 24 HpSC-HCC cases, EpCAM staining was very heterogeneous with a mixture of $EpCAM^+$ and $EpCAM^-$ tumor cells in each tumor (Fig 1F, **left panel**). Noticeably, many of the $EpCAM^+$ tumor cells were located at the invasion border zones and were often disseminated at the invasive front (black arrows). Immunofluorescence (IF) analysis revealed that HCC cells located at the invasive front co-expressed EpCAM, CK19, and AFP (Fig 1F, **right panels**). Noticeably, HpSC-HCC patients were significantly younger than MH-HCC patients (Suppl Tables 3-4). Enrichment of $EpCAM^+$ AFP^+ tumor cells at the tumor invasive front suggested their involvement in HCC invasion and metastasis.

Isolation and characterization of EpCAM$^+$ cells in HCC

The results above suggest that HpSC-HCC may be organized in a hierarchical fashion in which EpCAM$^+$ tumor cells act as stem-like cells with an ability to differentiate into EpCAM$^-$ tumor cells. To test this hypothesis, we first evaluated the expression pattern of seven hepatic stem/maturation markers (EpCAM, CD133, CD90, CK19, Vimentin, Hep-Par1, and β-catenin) in six HCC cell lines (Fig 2A). All three AFP$^+$ cell lines (HuH1, HuH7, and Hep3B) expressed EpCAM, CD133, and cytoplasmic/nuclear β-catenin, whereas the other three AFP$^-$ cell lines (SK-Hep-1, HLE, and HLF) did not, consistent with the microarray data. Interestingly, AFP$^+$ cell lines had no CD90$^+$ cell population which was recently identified as hepatic CSCs [35], whereas AFP$^-$ cell lines had such a population. Consistently with the IF data, FACS analysis showed that AFP$^+$ cell lines had a subpopulation of EpCAM$^+$ and CD133$^+$ but no CD90$^+$ cells, whereas AFP$^-$ cell lines had a subpopulation of CD90$^+$ cells but no EpCAM$^+$ nor CD133$^+$ cells (Fig 2B). These data indicate that HpSC-HCC and MH-HCC cell lines have distinct stem cell marker expression patterns, and EpCAM as well as CD133 may be hepatic CSC markers specifically in HpSC-HCC.

We selected two human HCC cell lines (HuH1 and HuH7) to isolate EpCAM+ cells since both lines were heterogeneous in EpCAM, AFP, CK19 and β-catenin expression (Fig 2A-B and Suppl Fig 1A) [29]. We successfully enriched EpCAM$^+$ and EpCAM$^-$ populations from HuH7 cells by fluorescence activated cell sorting (FACS), with >80% purity in EpCAM$^+$ cells and >90% in EpCAM$^-$ cells one day after sorting (Fig 3A). Similar results were obtained when the purity check was done immediately post-sorting (data not shown). EpCAM$^+$ cells were also positive for CK19 and β-catenin (Fig 3B and Suppl Fig 1B) and most were AFP$^+$ (data not shown). In contrast, EpCAM$^-$ cells were negative for these markers but positive for HepPar1, a monoclonal antibody specific to hepatocytes (Fig 3B). Consistent with the microarray data described above, the levels of *TACSTD1, MYC* and *hTERT* (known HpSC markers) were significantly increased in EpCAM$^+$ HuH7 cells, while the levels of *UGT2B7* and *CYP3A4* (known mature hepatocyte markers) were significantly higher in EpCAM$^-$ HuH7 cells (Fig 3C, **left upper panel**). This expression pattern was reminiscent of human HpSC cells (Fig 3C, **left lower panel**). Similar results were obtained from HuH1 cells (data not shown). We also compared gene expression patterns of isolated HuH1, HuH7, MH and HpSC cells using the TaqMan® Human Stem Cell Pluripotency Array containing 96 selected human stem cell-related genes. Although a differential expression pattern of stem cell related genes was evident among HpSC, EpCAM$^+$ HuH1 and EpCAM$^+$ HuH7 cells, EpCAM$^+$ HCC cells were more closely related to HpSC cells while EpCAM$^-$ HCC cells were more closely related to diploid adult mature hepatocytes (Fig 3C **right panel**, Suppl Fig 1C). Thus, it appeared that EpCAM$^+$ HCC cells had a gene expression pattern that is more closely related to HpSC than EpCAM$^-$ HCC cells.

The isolated EpCAM$^+$ HuH7 cells formed colonies efficiently while EpCAM$^-$ cells failed to do so (Fig 3D **upper and middle panel, and** Suppl Fig 2A **for HuH1 cells**). In addition, EpCAM$^+$ HuH7 cells were much more invasive than EpCAM$^-$ cells ($P < 0.03$) (Fig 3D **lower panel and** Suppl Fig 2B **for HuH1 cells**). The EpCAM$^+$ fraction decreased with time in sorted EpCAM$^+$ HuH7 cells from >80% to 50% (Fig 3E). However, a small percent of EpCAM$^+$ cells remained constant in sorted EpCAM$^-$ HuH7 cells. FACS analysis confirmed the results of IF analysis (Fig 3F and Suppl Fig 2C **for HuH7 and HuH1 cells, respectively**), suggesting that EpCAM$^+$ cells could differentiate into EpCAM$^-$ cells, eventually allowing an enriched EpCAM$^+$ fraction to revert back to parental cells after 14 days of culture. In contrast, EpCAM$^-$ cells maintained their EpCAM$^-$ status. In addition, we successfully isolated 12 HuH1 and 2 HuH7 colonies from 192 single cell-plated culture wells. However, all colonies were heterogeneous in EpCAM and AFP expression and no colony was completely EpCAM$^-$ (data not shown). Taken together, these results indicate that EpCAM$^+$ HCC cells resemble HpSC